Reviews in Mineralogy & Geochemistry
Vol. 78 pp. 1-31, 2014

Modern X-ray Diffraction Methods in Mineralogy and Geosciences

Barbara Lavina

High Pressure Science and Engineering Center
and
Department of Physics and Astronomy
University of Nevada
Las Vegas, Nevada 89154, U.S.A.

lavina@physics.unlv.edu

Przemyslaw Dera

Hawaii Institute of Geophysics and Planetology
School of Ocean and Earth Science and Technology
University of Hawaii at Manoa
1680 East West Road, POST Bldg, Office 819E
Honolulu, Hawaii 96822, U.S.A.

Robert T. Downs

Department of Geosciences
University of Arizona
Tucson, Arizona 85721-0077, U.S.A.

INTRODUCTION

A century has passed since the first X-ray diffraction experiment (Friedrich et al. 1912). During this time, X-ray diffraction has become a commonly used technique for the identification and characterization of materials and the field has seen continuous development. Advances in the theory of diffraction, in the generation of X-rays, in techniques and data analysis tools changed the ways X-ray diffraction is performed, the quality of the data analysis, and expanded the range of samples and problems that can be addressed. X-ray diffraction was first applied exclusively to crystalline structures idealized as perfect, rigid, space and time averaged arrangements of atoms, but now has been extended to virtually any material scattering X-rays. Materials of interest in geoscience vary greatly in size from giant crystals (meters in size) to nanoparticles (Hochella et al. 2008; Waychunas 2009), from nearly pure and perfect to heavily substituted and poorly ordered. As a consequence, a diverse range of modern diffraction capabilities is required to properly address the problems posed. The time and space resolution of X-ray diffraction now reaches to nanoseconds and tens of nanometers. Time resolved studies are used to unravel the mechanism and kinetics of mineral formation and transformations. Non-ambient conditions such as extreme pressure and temperature are created in the laboratory to investigate the structure and properties of the Earth's deep interior and the processes that shape the planet.

This chapter is not intended to be comprehensive or detailed, because diffraction is such a vast subject. We will, however, summarize the principles of diffraction theory under the assumption that the reader is familiar with basic concepts of the crystalline state. We will

1529-6466/14/0078-0001$05.00 http://dx.doi.org/10.2138/rmg.2014.78.1

briefly review the basics of diffraction techniques, using laboratory and synchrotron X-ray sources and highlight some of their applications in geoscience. For briefness, we will omit the discussion of structure solution as most of experiments in the geosciences are performed on materials of known structure.

General resources for crystallographers include the International Tables for Crystallography (2006), a comprehensive learning and working resource including symmetry and properties of crystals, theory and practice of most techniques as well as tables of symmetry elements and mathematical, physical and chemical parameters. A thorough presentation of the theory of diffraction can be found in Fundamentals of Crystallography (Giacovazzo 2011), while other noteworthy books include Boisen and Gibbs (1985), Stout and Jensen (1989), Warren (1990), Ladd and Palmer (2003), Blake and Clegg (2009), and Glusker and Trueblood (2010). The websites CCP14 and SINCRIS list and link most of the available crystallographic software; useful crystallographic tools can be found at the Bilbao Crystallographic server (Aroyo et al. 2006a,b). Crystal structure databases of minerals include the open access American Mineralogist Crystal Structure Database (Downs and Hall-Wallace 2003), and the Crystallographic and Crystallochemical Database for Minerals and their Structural Analogues of the Russian Academy of Science (MINCRYST, Chichagov et al. 2001). Resources for inorganic crystal structures in general include the Crystallographic Open Database (Gražulis et al. 2012), the Inorganic Crystal Structure Database (ICSD) and the Cambridge Structural Database (CSD).

GENERAL ASPECTS

Brief introduction to X-ray diffraction theory

Most X-ray diffraction techniques rely exclusively on the portion of X-rays elastically scattered by electrons (Thomson scattering). The diffraction event can be visualized as a consequence of the interaction between electromagnetic radiation and electrons. The electromagnetic radiation enters the material with a certain frequency and the electrons in the material "ride the waves", oscillating in the direction of the polarization of the incident light. Since an accelerating electron in turn creates electromagnetic radiation, the oscillating electrons in the material give off light in spherical distributions, all with the frequency of the oscillating electrons. The transfer of energy from the incident light into the oscillation of the electrons takes place by decreasing the intensity of the incident X-rays. In order for X-rays to be diffracted, namely to be spherically scattered and then experience constructive interactions in particular directions, they have to interact with a material showing a periodicity in the distribution of electrons comparable to the X-ray wavelength (λ). The wavelength of X-rays, ranging from 0.1 to 100 Å (equivalent to energies of about 120 to 0.1 keV) is in the range of interatomic distances or unit cell sizes, and therefore diffraction can be produced by the elastic interaction of X-rays with matter having some degree of ordering.

X-rays are scattered by electrons, and as a consequence the scattering power of an atom is correlated to its number of electrons. Due to the interference between scattered waves from different portions of the electronic cloud of an atom, the effective scattering intensity, or scattering factor, decreases with the scattering angle (Fig. 1). Interference effects are greater with increasing distance from the atom center; outer-shell electrons contribution to the scattered wave decreases more rapidly in comparison to inner electrons contribution with increasing scattering angle. For most applications, the distribution of electrons around nuclei is considered spherical, and so is the scattering factor. Tables of the calculated scattering factors for neutral atoms ideally at rest can be found in Brown et al. (2006b). Atoms constantly vibrate about their equilibrium positions. The amplitudes of vibration have two components, there is a quantum effect, known as zero-point motion, due to the uncertainty principle, while

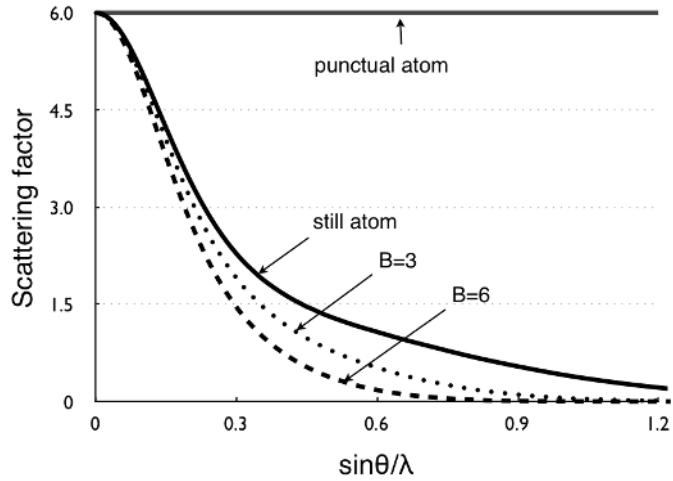

Figure 1. The atomic scattering factor for an ideal point-like atom is constant. The volume of a real atom, however, causes the scattering factor to decrease substantially with the scattering angle (solid curve), an effect that is increased for atoms in motion as shown by dotted curves calculated for two values of the displacement parameter B.

above 0 K atoms undergo thermal vibrations around their average positions (Downs 2000). Furthermore, different atoms, e.g., Si and Al, may occupy a single crystallographic site but in slightly different locations, and this creates a smear in the average electron density known as static displacement. Static and dynamic disorders are represented in the description of a crystal structure with atomic displacement parameters (ADP). The positional disorder of an atom, whether static or dynamic, has the effect of increasing the average volume of the electron cloud and therefore decreases the scattering amplitude (Fig. 1). For practical purposes, the most important facts related to the scattering factors are: i) the Z dependence of the scattering power makes atoms with similar atomic numbers virtually undistinguishable by means of X-ray diffraction; ii) the diffracted signal decreases with the scattering angle, therefore X-ray diffraction peaks at high scattering angles are on average weak; iii) the latter effect is increased by static and dynamic positional disorder.

Bragg's description of diffraction by a crystal, although not physical, is useful to explain X-ray diffraction in an intuitive way and to provide a mathematical method for computing diffraction directions. In Bragg's representation, diffraction is described as the reflection of an X-ray beam by crystallographic planes defined by indices *hkl*. Incident waves reflected by equivalent planes with characteristic separation d_{hkl} are in phase if the difference in their travel (2Δ in Fig. 2) is equal to an integral number of wavelengths, *n*:

$$2d_{hkl}\sin\theta_{hkl} = n\lambda \tag{1}$$

The *d*-spacing of the set of planes generating a diffraction peak may be easily calculated from observed diffraction angles, provided the wavelength is known, using the Bragg equation. The minimum *d*-spacing measured in an experiment defines the resolution. From Bragg equation, it appears that if an experiment imposes small maximum 2θ, as is often the case in non-ambient experiments, the use of incident radiation with short wavelength improves the resolution.

A very useful representation of the translational symmetry of a crystal is given by the reciprocal lattice, which is derived from the direct lattice as the set of vectors with directions normal to lattice planes (*h k l*) and lengths of $1/d_{hkl}$. The reciprocal lattice allows a simple

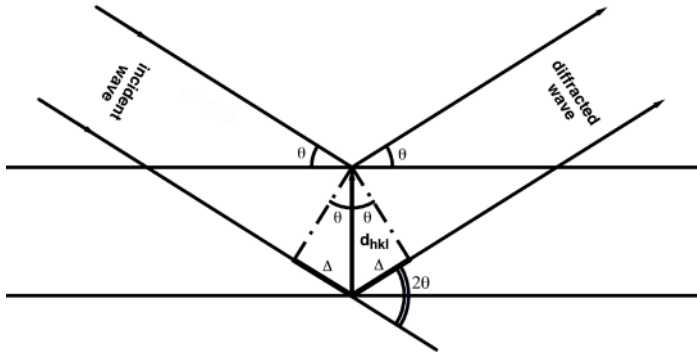

Figure 2. Bragg's representation of the diffraction condition as the reflection of X-rays by lattice planes (*h k l*).

visualization of diffraction conditions by the Ewald construction (Ewald 1921) shown in Figure 3. The origin of the reciprocal lattice (*O*) is set at the intersection of a sphere of radius 1/λ, the Ewald sphere, with the incident beam passing through the center of the sphere (*C*). It is easy to verify that for any reciprocal vector intersecting the Ewald sphere, the angle at the vertex of the isosceles triangle $O\hat{C}R$ in Figure 3 equals 2θ, and therefore Bragg's equation, i.e., the diffraction condition, is satisfied when a reciprocal lattice node intersects the Ewald sphere. Using Ewald's sphere we can readily notice that the wavelength defines the maximum resolution: $d^*_{max} = 1/d_{min} = 2/\lambda$, the sphere of radius 2/λ is indeed called the limiting sphere. The value of $d^*_{max} = 2/\lambda$ is imposed by Equation (1) since the scattering angle cannot exceed $2\theta = 180°$.

The intensity of a diffracted beam is a function of the technique (formulation for powder and single crystal monochromatic techniques will be given later), instrumental parameters (e.g., intensity of the source) and composition and crystal structure of the specimen. As mentioned earlier, the objects scattering X-rays are electrons, and so it follows that the intensity of a diffracted beam depends on the electron density distribution within the crystal. In ordered (in

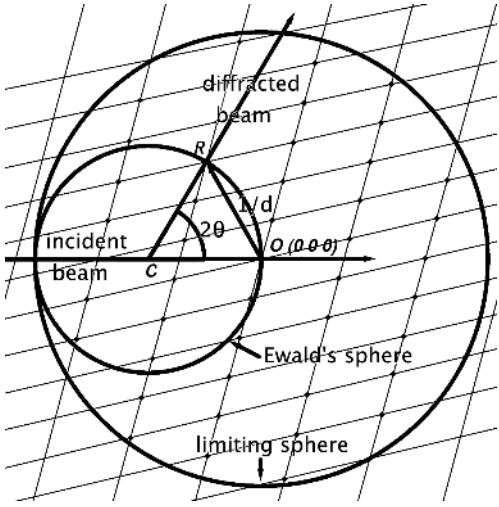

Figure 3. Ewald representation of the diffraction condition. O: origin of the reciprocal lattice, C: center of the Ewald sphere, R: reciprocal node positional vector of length 1/*d*. Only the nodes of the reciprocal space falling within a radius 2/*d* may be placed, upon crystal rotation, on the surface of the Ewald sphere and be measured.

a crystalline sense) materials, only the electron density within the asymmetric part of the unit cell needs to be considered and it can be represented with a set of atomic positions, scattering factors and displacement parameters. The scattering power of a crystal in the direction of a diffraction peak is given by the structure factor, $\boldsymbol{F}_{hkl}$:

$$\boldsymbol{F}_{hkl} = \sum_{j=1}^{N} f_j e^{2\pi i(\vec{h}\cdot\vec{r})} = \sum_{j=1}^{N} f_j \exp\left[2\pi i\left(hx_j + ky_j + lz_j\right)\right] \tag{2}$$

where *hkl* are the reflection indices, *j* indicates an atom in the unit cell with scattering factor f_j (which includes thermal vibrations), *i* is the imaginary number, $\vec{h}$ and $\vec{r}$ are the interplanar vector and the positional vectors, and *x, y, z* are the atomic fractional coordinates. The complex term $2\pi i(hx_j + ky_j + lz_j)$ may be viewed as the difference in phase between the atomic position and the origin of the unit cell. The electron density distribution may be calculated from values of the structure factors through Fourier transform. However, because only the amplitude of the scattering factors and not their phase can be measured, the electron density map of an unknown structure cannot be simply calculated from its diffraction pattern (the phase problem in crystallography).

Ideal structures, real structures, liquids

Nature offers many examples of large, nearly pure and perfect gems of astonishing beauty, usually grown in rather unique environments over long time periods. The vast majority of minerals, however, contain a high concentration and variety of defects that appear wonderful to the eye of a geoscientist because of the wealth of information they bear. Defects have an important contribution in a crystal energetics; they are typically strongly affected by the history of a mineral and, as such, are an important part of the geological record (Putnis 1992; Ottonello 1997). Defects strongly affect mineral properties, including color, crystal form, reactivity, diffusion, mechanical strength, thermal conductivity and electronic properties. Some widespread materials, such as clays and hydroxides, rarely grow in grains large enough to produce a "good powder pattern." Furthermore, interstitial water and cations are typically highly variable from particle to particle and within particles, generating variability in site occupancies and layer stacking disorders. In contrast, amorphous materials and liquids usually display short range ordering where interatomic distances show a spherical distribution that rapidly randomizes beyond a few bond lengths. We will show later that these materials can also be explored by means of X-ray diffraction.

Common structural defects in minerals include twinning, vacancies and interstitials, chemical substitutions, chemical disorder among crystallographic sites, dislocations and stacking faults. Recently, natural quasicrystals have been discovered (Bindi et al. 2009; Steinhardt and Bindi 2012). Structural defects may be randomly distributed in a crystal or may be clustered or periodically distributed with very different effects on diffraction patterns. Defects formed in a crystal at high temperature may achieve an ordered distribution upon cooling, eventually forming a modulated structure resulting in "extra" peaks in diffraction patterns compared to random distributions. Defects can be pictured as disruption of the ideal symmetry, therefore, like a distorted or damaged mirror, they cause a reduction in the "phasing power" of a lattice, it is therefore intuitive that they have the effect of decreasing or broadening the Bragg peaks and produce scattering in between Bragg peaks. Structural defects show a different degree of ordering; the lower the degree of ordering, the more diffuse is its associated scattering. Defects generate superstructure and satellite reflections, diffuse lines and planes and more or less isotropic diffuse scattering. Different diffraction methods are employed to investigate defects, which often require high resolution in order to emphasize weak features such as the diffuse scattering. The modeling required for the interpretation of defect structures and their diffraction effects changes with the degree of ordering. Vacancies, interstitials and modulated structures, twins and stacking fault structures can still be described in terms of unit

cell parameters and atomic coordinates, in a 4 or higher dimensions space. Consequently, the diffraction effects of such defects can be described with the same theory of diffraction used for perfect crystals. For amorphous and liquid phases or highly disordered materials such as clays, a generalized theory of diffraction is adopted and will be briefly presented later. Among books dedicated to the characterization of defect structures we mention Billinge and Thorpe (1998), Snyder and Bunge (2000) and Frey et al. (2010).

Information obtained from X-ray diffraction experiments

Having reviewed the principles of X-ray diffraction, we now summarize the information that may be derived from diffraction experiments and how it can relate to geoscience problems. If samples of good crystallinity and suitable instruments are available, X-ray diffraction can provide structural information of very high precision and accuracy. We recall that the information is averaged over the volume of the illuminated sample and is not element-selective (with the exception of resonant diffraction techniques). For instance, most X-ray diffraction techniques cannot discriminate between a site occupied entirely by silver and a site occupied by equal amounts of palladium and cadmium because the total number of electrons is the same in both cases. Spectroscopic data, displacement parameters and bond lengths considerations are therefore complementary to X-ray diffraction. In contrast, structural parameters from diffraction analysis are often indispensable information in the interpretation of spectroscopic results.

The combination of diffraction angles and intensities is characteristic of a mineral, and therefore constitute a powerful tool for phase identification through search/match routines using crystallographic databases. It is also possible to perform an estimation of phase abundances through whole profile fitting of powder diffraction data.

From the geometrical distribution of diffraction effects (diffraction angles) the geometry of the crystal lattice, its orientation, and the unit cells parameters *a, b, c*, α, β, γ can be determined. Lattice parameters not only represent a fundamental component in the structural characterization of a material, but from these a wealth of geologically relevant information may be derived. Provided the composition is known, the mineral density may be calculated, a parameter essential to the modeling of the Earth's interior and processes such as the segregation of crystals in magma and planetary differentiation. The determination of lattice parameters as a function of pressure and temperature provides important thermodynamic parameters such as bulk and linear compressibility and thermal expansion. Materials of the Earth may experience immense non-hydrostatic stresses (orogenesis, earthquakes, meteorite impacts etc.), resulting in lattice deformations that depend on pressure, temperature, grain size, orientation and material properties. Strain is measured *in situ* by producing controlled stress and measuring the deformation. Residual strain is measured in natural samples with the purpose of reconstructing the history and value of the stress tensor, estimate the size and velocity of an extraterrestrial object impacted on Earth, or to determine the origin of a mineral. The lattice preferred orientation in a rock (widely studied by electron microscopy except for in situ investigations) usually determines the rock anisotropy.

Diffraction intensities, as mentioned earlier, depend on the atomic arrangement and static or dynamic displacements of atoms. The structural solution is the process of assigning the atomic distribution in the unit cell. Structure refinement produces accurate atomic positions, site occupancies and displacement parameters, typically determined through an iterative process of least-squares minimization of the differences between observed and calculated structure factors. Structure factors are obtained from the intensities of the diffraction peaks, and are mathematically related to the structural model. Results of structural refinement can be used to interpret bulk properties in terms of atomic structure; for instance, the bulk compressibility of a silicate can be understood in terms of differential bond compressibility and bridging Si-O-Si

angle bending. The determination of the coordination numbers and bond distances is crucial in understanding isomorphic substitutions and consequently processes such as differentiation, ore formation and so forth. Experimental site occupancies give the intracrystalline atomic distribution of binary solid solutions as long as atomic species differ sufficiently in atomic number. The systematic characterization of mineral structures leads to the development of predictive models of the crystal chemistry of minerals and empirical trends in the behavior of minerals (Hazen and Finger 1982).

Some of the main weaknesses of X-ray diffraction are related to the Z-dependency of atomic diffraction power. Parameters of light (low atomic number) elements can be difficult to determine particularly when the sample also contains heavy elements, because the contribution of the stronger scatterers dominates the signal. Furthermore the information derived from an X-ray experiment is an average over the illuminated volume, it makes no difference in most techniques if substituting elements are clustered in neighbor unit cells or are randomly distributed.

X-ray: characteristics, sources, choice

X-ray sources differ substantially in power, energy (wavelength), beam geometry and tunability. An X-ray source is described by its intensity (photons/sec), collimation (angular divergence), beam size, spectral distributions, and time structure. A quantity commonly used to characterize an X-ray source is the brilliance:

$$brilliance = \frac{intensity}{divergence \times area \times bandwidth} \tag{3}$$

in which the intensity is usually expressed in photons/seconds, the divergence in mrad^2, the area in mm^2, the bandwidth, describing the spectral distribution, is expressed in 0.1%. Several orders of magnitude separate the brilliance of laboratory sources from synchrotrons and these from free-electron lasers (Fig. 4).

Laboratory sources include sealed tubes and rotating anodes. In both devices a metal target is bombarded with a beam of electrons accelerated by a high electrical potential applied between the filament emitting electrons and the target. The interaction between the electron beam and the target's electrons include collision, excitation and de-excitation events that generate X-ray emissions composed of a white radiation spectrum and few strong peaks of characteristic wavelength dependent on the material used. The wavelength (λ) of the characteristic radiation is given by Moseley's Law:

$$\frac{1}{\lambda} = c\left(Z - \sigma\right)^2 \tag{4}$$

where c and σ are constants and Z is the atomic number. In most laboratory instruments, the inner energy level "K_α" characteristic wavelength is selected using a monochromator. Most common target materials are molybdenum and copper with characteristic average K_α wavelengths of 0.7107 and 1.5418 Å respectively; other target metals such as Ag and Au are used for applications requiring higher energy. X-ray laboratory sources are in continuous development; we recommend consulting vendor websites for the latest updates in laboratory sources. The performances of laboratory sources differ considerably in flux, and in the focusing size from about 1 mm to about 0.05 mm. The radiation is unpolarized and spherically divergent.

Large user facilities, storage rings and free electron lasers, provide radiation of very high brilliance and properties tunable over a very wide range. Synchrotron radiation is generated when charged particles traveling at relativistic speed are accelerated. User-dedicated sources of synchrotron radiation are storage rings of diameter up to about 2 km where a small, high

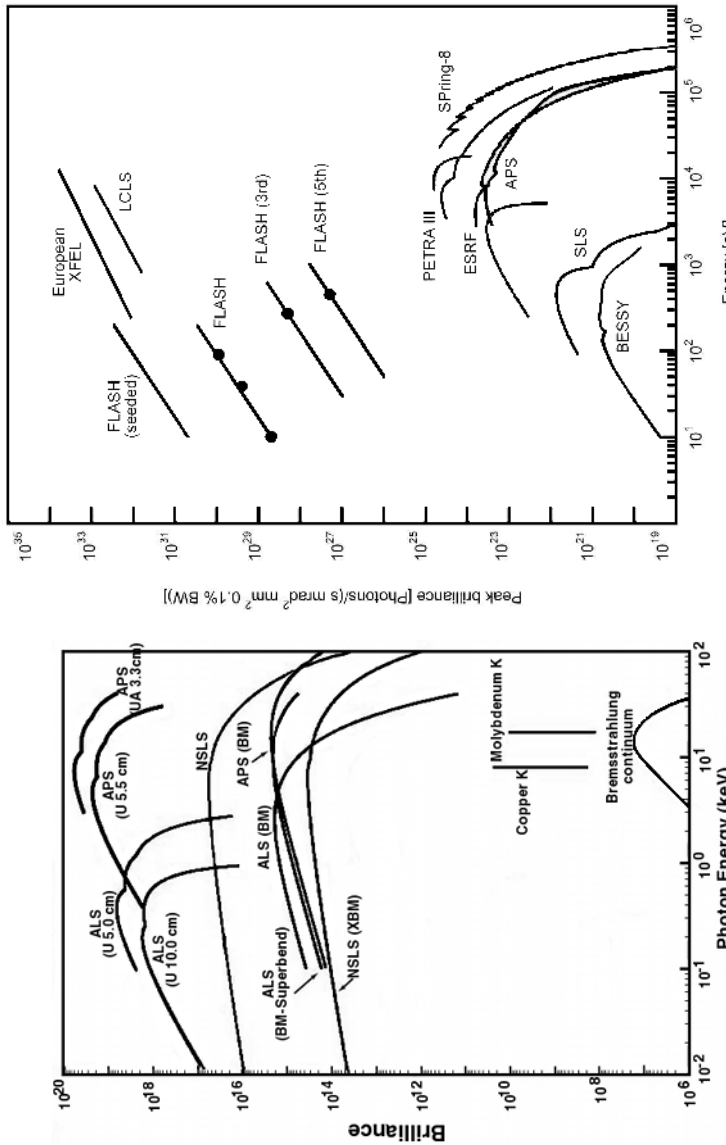

Figure 4. These figures compare the brilliance of storage rings sources with laboratory sources (*left*, Argonne National Laboratory) and storage rings sources with free electron laser sources (*right*) as a function of energy.[Right figure modified and used with permission of IOP Science from Robinson et al. (2010) *New J Phys*, Vol. 12, Fig. 1, p. 2.]

energy, pulsed electron beam travels at relativistic speed in a closed path. The energy of a storage ring reaches 8 GeV (Spring-8, Japan) in third generation synchrotrons; the beam size is of the order of tens to hundreds of μm, the bunch length is of the order of tens of ps. Because of relativistic effects, a broad spectrum light is emitted when charged particles traveling at such speed are accelerated, in a synchrotron this happens as a result of the magnets used to curve the beam trajectory (curved sections of the ring) and in insertion devices (straight sections of the ring). Bending magnet sources are characterized by a broad spectrum. Insertion devices contain an array of magnets of alternate fields causing the electron beam to oscillate in the horizontal direction. In wigglers the oscillations are relatively large and the light produced at each oscillation sums up incoherently, the effect is to greatly increase the total power of the beam, which still displays a broad spectral range. Undulators are designed to obtain coherent interactions between the light emitted at each oscillation, this occurs for a particular wavelength and its harmonics only; the emitted beam has reduced angular divergence and is composed of a few intense peaks with a much higher brilliance compared to bending magnets and wigglers. The characteristic wavelength of an undulator can be tuned by changing the intensity of the magnetic field. X-ray optics are used to monochromatize and focus the beam to a wide range of sizes. Monochromatization is achievable down to meV and focusing can be brought down to tens of nm. A synchrotron hosts a large number of beamlines, equipped with different insertion devices and X-ray optics to customize the experimental stations with the radiation most suitable for a given technique and type of experiments.

X-ray free-electron lasers (FEL) generate much brighter and shorter pulsed X-rays compared to synchrotrons (Fig. 4). A few are under construction; the Linac Coherent Light Source (LCLS, Stanford) is the first facility available to the user community. FEL radiation sources have the power to "see" single atoms and to resolve in time processes such as the bond formation: observations fundamental to the nature of materials that may affect science broadly. One of the applications relevant to planetary science is ultrafast diffraction on samples under pressures and temperatures of the interior of giant planets in laser generated shock events. Useful introductions to synchrotron and FEL radiations and their applications include Margaritondo (1988, 2002), Brown et al. (2006a), Sutton (2006), Als-Nielsen and McMorrow (2011), and Lee (2011).

Finally, efforts have been made to develop sources for portable diffractometers for field-work and extraterrestrial exploration (Bochenin 1973; Sarrazin et al. 1998, 2005; Yamashita et al. 2009; Hansford 2011) such as the CheMin instrument installed in the 2012 Mars Rover (Blake et al. 2009).

Selecting the proper X-ray source is critical to the success of an experiment. The choice of the source depends on materials, techniques, and type of experiment. Laboratory sources are routinely used in geoscience for a wide range of experiments, from phase identification to high resolution non-ambient studies. Compared to central research facilities such as synchrotrons, where time allocated for individual experiments is very limited (typically a few hours to a few days), laboratory X-ray diffraction instruments have much less time restrictions, which can be used to tune and optimize the data collection conditions. The high brilliance of synchrotron radiation is essential to perform experiments on very small samples and weak scatterers, for ultra-fast time-resolved studies, where highly focused radiation is required to reduce scattering effects from the environmental cell, for high resolution mapping, or when high energy or specific wavelengths are necessary. The drawbacks of using synchrotron radiation are mostly related to the limited time available, the traveling costs, and less standardized data collection and processing procedures compared to laboratory sources. Accurate planning of an experiment is critical to its success. In general, there is no cost associated with running the experiment, as these costs are usually absorbed by the agency that funds the facility.

X-RAY DIFFRACTION TECHNIQUES

Single crystal monochromatic diffraction (SXD)

Single crystal monochromatic diffraction is a very mature technique described in details in several books, including Stout and Jensen (1989), Clegg (2001), Ladd and Palmer (2003), Dauter and Wilson (2007), Glusker and Trueblood (2010). As shown in Figure 3, for an arbitrary orientation of a crystal in a monochromatic X-ray beam, it is highly unlikely that more than a few reciprocal space nodes fall on the Ewald sphere and therefore, satisfy the reflection condition, and generate Bragg peaks. In order to measure a sufficient portion of reciprocal space, a crystal must be rotated to bring more vectors into the diffraction condition. If a large area detector and short wavelengths are used, it might be sufficient to rotate the crystal along a single axis (rotation method). The output of a typical SXD data collection consists of a peak list, including indices, diffraction angles, integrated intensities and their standard deviations. If an area detector is used, then the peak positions (directions of diffracted beams) are represented by detector pixel coordinates, whereas with a point detector, all diffraction events occur in the detector plane (usually horizontal) and the detector angle is sufficient. Angles are used to determine unit cell parameters, while intensities are used to determine the average atomic arrangement in a crystal.

Measurements. The essential parts of a single crystal diffractometer are a monochromatic X-ray source, a goniostat, a detector and computer control. Most laboratory diffractometers use Mo K_α radiation (with two spectral components $K_{\alpha1}$ and $K_{\alpha2}$) which provides sufficient resolution. Rotations are realized with Eulerian cradles or kappa goniostats with a variable number of circles. The greater the number of circles the greater the flexibility in sample and detector positioning, which is particularly useful when environmental cells are used. The precision of goniostats is given by the sphere of confusion (SoC): the minimum spherical volume covering all possible locations of an infinitely small object at all possible goniometer orientations (Davis et al. 1968). High precision goniostats are required when small crystals are studied with beams of comparable size. Point (scintillator-based) and area detectors (CCD, image plate, etc.) are used in SXD. A point detector can be collimated (narrow slits are positioned in front of the detector to block radiation coming from directions other than the sample), which is particularly useful in case of high background. Furthermore a point-detector data collection can be programmed to modify the speed according to peak intensities, improving the statistics of weak reflection measurements by increasing $I/\sigma(I)$. This is an important advantage, considering that the range of intensities of SXD peaks typically exceeds the linear range of most detectors. Area detectors have the advantages of being fast, and allow the whole integrated peak intensity to be recorded in one exposure, while a profile is usually measured in step-scan mode with a point detector. Area detectors record whole portions of reciprocal space, including off-Bragg intensities. In this way, diffuse scattering or satellite peaks, that might be overlooked when point detectors are used, can also be recorded.

Sample choice, peak search and indexing. Sample crystals should be carefully selected using a microscope. Crystals without inclusions, of euhedral shape and with sharp extinction are more likely to be unstrained single crystals. Depending on sample scattering power and source intensity, crystals of roughly 50 to 500 μm in diameter can be measured with laboratory instruments while smaller samples, down to below 1 μm in size, are measured using synchrotron radiation. The crystal is positioned at the instrument center (intersection of the rotation axes) on the beam path. The measurement proceeds with a search for reflections, an operation that might require a few hours with a point detector. A first evaluation of the crystal quality is based on peak shapes. “Good crystals” show narrow, symmetric peak profiles. If the unit cell of the crystal is approximately known, with at least two, but usually not less than 5, non-coplanar reciprocal vectors (peaks) a lattice can be defined, and using mathematical tools the conventional cell may be derived, this allows the calculation of an orientation matrix and

indexing of the peaks. The presence of peaks that cannot be indexed is usually an indication of multiple crystals or twins. The initial matrix is used to predict peak positions and define the data collection strategy. This consists of sets of reflections with calculated angular positions if a point detector is used. With area detectors, a set of rotations/step scans that allow the exploration of a large portion of reciprocal space is collected.

Lattice parameters. The accurate determination of lattice parameters is critical in mineralogy. Lattice parameters are determined by least-squares refinements against peak angles or *d*-spacings, imposing symmetry constraints when appropriate. The full list of measured reflections is used in the least-squares refinement when a 2D area detector is used. With point detectors, a short peak list of particularly carefully chosen reflections is used. The "8-position centering method" (King and Finger 1979), described in detail by Angel et al. (2000), consists of measuring one or more reflections at 8 diffractometer positions at opposite diffraction angles to compensate for instrumental and centering errors provides the basis for a very precise lattice parameter determination.

Diffraction intensities and data reduction. Peak intensities are measured by swiping nodes of the reciprocal space through the Ewald sphere (Fig. 3). Unlike the ideal geometric points, nodes of the reciprocal lattice have a volume determined by the crystal shape and mosaicity; in order to collect meaningful intensities the entire volume of the nodes must cross through the Ewald sphere at constant speed. The expression linking experimental integrated intensities with the structure factors assumes the following form in SXD:

$$I(hkl) = I_0 \frac{\lambda^3}{V_{\text{cell}}^2} \left(\frac{e^2}{mc^2} \right) V_{\text{cr}} LPTE\left[F(hkl)\right]^2 \tag{5}$$

where I_0 is the intensity of the incident beam, λ is its wavelength, e, m, c are universal constants, V_{cell} and V_{cr} are the volume of the unit cell and of the crystal, L, P and T are the Lorentz, polarization and transmission factors, E is the extinction coefficient. The process of deriving observed structure factors from experimental intensities by estimating the above terms is called data reduction. The L, P, T and E factors differ from peak to peak in SXD; the proper evaluation of these corrections is essential to obtain high quality structural analysis. The Lorentz factor is a technique-dependent parameter that accounts for the time required for reflections to cross the Ewald's sphere. Algorithms for the calculation of the L factor are given in the literature (Lipson et al. 2006) and are implemented in most commercial diffractometers. The polarization factor is a function of the polarization of the incident beam and the scattering angle. For non-polarized beam, in the case of conventional source, P is given by $P = (1 + \cos^2 2\theta)/2$. The fully polarized synchrotron radiation is slightly modified by the X-ray optics, algorithms for the calculation of P are given by Kahn et al. (1982); the magnitude of the polarization correction at synchrotrons is usually very small.

The transmission factor accounts for the attenuation of the incident and diffracted beam due to crystal absorption. For each reflection the paths of the incident and diffracted beam in the crystal differ, so does the transmission factor. Due to the systematic trends of X-ray attenuation factors with energy and atomic number (Chantler 2000), T is small for light-element samples measured with high energy radiation. It is customary to calculate the "μr" product to gauge the absorption correction, where μ is the X-ray absorption coefficient (Hubbell and Seltzer 2004) and r is the average crystal size. The absorption correction is considered negligible in standard data collections when $\mu r < 0.1$. There are different strategies for calculating the absorption correction: i) if the crystal shape is known (either a euhedral shape defined by face indices and the distance of the facet from the crystal center of gravity) the absorption correction is calculated exactly for every set of diffraction angles; ii) in the semi-empirical correction (North et al. 1968) a measurement of the attenuation is obtained by measuring the intensity of few peaks at different combinations of two angles (called ψ-scan, this azimuthal scan is

equivalent to moving the reciprocal space node on the surface of the Ewald sphere). Carefully chosen ψ-scan curves are then used to model the three dimensional absorption correction; iii) if the dataset contains a large number of redundant and symmetry equivalent reflections, an idealized crystal shape can be calculated through the minimization of the discrepancy among equivalent reflections.

Extinction includes the attenuation of the incident beam, as it travels in the crystal due to diffraction, and the effect of multiple diffraction within the crystal. *E* is usually significant only in low mosaicity specimens measured with fairly low energy radiation. The correction is usually performed within the structural refinement.

The quality of observed structure factors $\boldsymbol{F}_O$ is quantified by the ratio between the intensities uncertainties and their values:

$$R_{sigma} = \frac{\sum \sigma\left(F_O^2\right)}{\sum F_O^2} \tag{6}$$

and, in the case redundant reflections are measured, by the discrepancy among equivalent reflections:

$$R_{int} = \frac{\sum \left|F_O^2 - \overline{F}_O^2\right|}{\sum F_O^2} \tag{7}$$

where $\overline{F}_O$ is the average intensity of a set of equivalents; the summations are performed over all *i* reflections for which at least one equivalent have been measured.

Structural refinement. Due to instrumental limitations (angular limits determined by movement range, collision limits, detector size) and time constraints, only a portion of reciprocal space within the resolution limit is usually measured in SXD experiments. Because the reciprocal lattice has some degree of symmetry, at least the center of symmetry, it is actually not necessary to measure all peaks within Ewald sphere; nonetheless, collecting redundant reflections greatly enhances the accuracy and precision of the structural analysis.

Observed structure factors are the input information for structural solution and refinement. Popular computer programs include SHELX (Sheldrick 2008) and SIR (Burla et al. 2012). A structural refinement consists of minimization of the differences between observed and calculated structure factors, for instance:

$$\sum w\left(F_O^2 - F_C^2\right)^2 \tag{8}$$

where *w* is a weighting factor, which is related to the confidence of individual measurements. $\boldsymbol{F}_C$ structure factors are calculated based on a structural model defined through atomic parameters (coordinates, occupancies, and displacement parameters) that are the variables in the structural refinement. The figures of merit used to assess the quality of a refinement are:

$$wR_2 = \left\{\frac{\sum\left[w\left(F_O^2 - F_C^2\right)^2\right]}{\sum\left[w\left(F_O^2\right)^2\right]}\right\}^{\frac{1}{2}} \tag{9}$$

$$R_1 = \frac{\sum\left|\left|F_O\right| - \left|F_C\right|\right|}{\sum\left|F_O\right|} \tag{10}$$

$$Goof = \left\{ \frac{\sum \left[w\left(F_O^2 - F_C^2\right)^2 \right]}{\left(n - p\right)} \right\}^{\frac{1}{2}} \quad (11)$$

where n is the number of independent reflections observed and p is the number of refined parameters. Detailed discussion of these procedures is beyond the scope of this chapter; nonetheless, it is worth recalling that it is crucial to critically evaluate the output of crystallographic calculations and to understand whether or not the experimental data can constrain structural parameters to the desired accuracy. A rule of thumb is to have five or more independent reflections per refined parameter; a "solid" refinement will have disagreements between observed and calculated parameters that are randomly distributed with respect to different sets of reflections (weak and strong, high and low 2θ); it is important to examine the correlations between parameters (site occupancies and displacement parameters are, in many calculations, highly correlated because similar local electron density distributions can be modeled with different combinations of the two parameters).

Advantages. Commercial instruments and software offer highly automated data collection and reduction procedures. Nonetheless, SXD experiments are cumbersome and time consuming measurements compared to powder diffraction or Laue techniques. SXD has, however, advantages that make the technique irreplaceable in several applications. The advantages include: i) symmetry equivalents reflection and reflections having the same *d*-spacing do not overlap, as in powder measurements, reducing the possibility of incorrect interpretations; ii) subtle features such as weak diffuse scattering can be more easily identified, as will be shown in detail below; iii) high background and broad peaks, while affecting the overall quality of the data, do not correlate with structural parameters in the structural analysis; iv) compared to polychromatic techniques, the data reduction is rather simple. In summary, monochromatic SXD provides the best measurement of reciprocal space; therefore if crystals of suitable size are available, then SXD is the method of choice for structural determination of new minerals or new synthetic phases (e.g., Britvin et al. 2002; Berlepsch et al. 2003; Bindi et al. 2011; Tait et al. 2011; Zelenski et al. 2011), for the study of defect structures, the determination of accurate site occupancies, atomic displacement parameters (e.g., Nakatsuka et al. 1999) and electron density distributions. SXD, however, is not suitable for fast time resolved studies and is particularly challenging at non-ambient conditions.

Laue method

The Laue method is the oldest of the X-ray diffraction techniques and it offers the simplest setting with minimal instrumental requirements. The technique uses polychromatic radiation. The sample, composed of one or few crystals, is stationary and the diffracted pattern is collected with an area detector in transmitted or reflected geometry. In the Laue method, the diffraction condition is realized for all reciprocal nodes that, for the particular orientation of the crystal, fall in the volume included between the Ewald spheres of radii $1/\lambda_{max}$ and $1/\lambda_{min}$ (Fig. 5). Many reflections satisfy the diffraction condition simultaneously; a large, though incomplete, sampling of the reciprocal space is realized in a single exposure from a stationary crystal (Fig. 6). Because most X-ray area detectors do not discriminate amongst the energies of diffracted peaks, for a peak at a given 2θ only the ratio λ/d may be calculated, which makes indexing more challenging compared to monochromatic techniques. Furthermore, lattice parameters may be determined up to a multiplicative constant (relative lattice parameters). This problem can be overcome by collecting also a single monochromatic exposure (at available beamlines) so the absolute value of few *d*-spacing may be measured (Budai et al. 2008). Alternatively, in the quasi-Laue technique, multiple diffraction patterns are collected while scanning the energy of the beam, so the Laue image is obtained as a series of single variable energy images

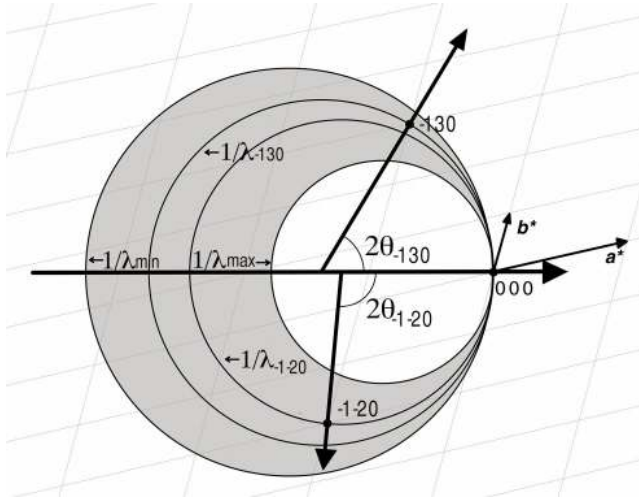

Figure 5. Two dimensional representation of diffraction in the Laue method. The node of the reciprocal lattice for a given crystal orientation that fall in the volume enclosed by the $1/\lambda_{max}$ and $1/\lambda_{min}$ spheres (grey area) diffract intermediate energies.

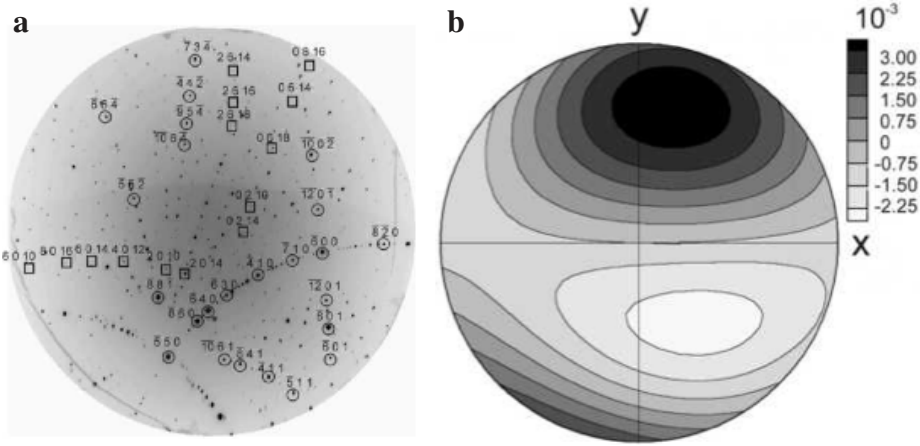

Figure 6. a) Example of a Laue diffraction pattern obtained from a magnetite crystal (squares) embedded in plagioclase (circles) and b) strain tensor in polar coordinates for the same sample of magnetite. Unit of contour are micro-strain (Wenk et al. 2011).

(Wang et al. 2010). If structural refinement is the goal of the experiment, then reciprocal space needs to be sampled with sufficient coverage. In this case, patterns are collected at different angles by rotations perpendicular to the beam. Compared to monochromatic data collection, the data reduction requires additional terms including harmonic deconvolution and intensity normalization to account for the energy dependence of the intensity of the incident spectrum, the diffraction efficiency, the crystal absorption and the detector efficiency (Srajer et al. 2000). For these reasons, Laue diffraction is not commonly the technique of choice for structural determinations but yet a viable option (Ren et al. 1996, 1999; Yang et al. 1998; Srajer et al. 2000). The Laue technique takes advantage of the full energy spectrum of an X-ray source. A remarkable advantage of the technique is that the sample can be stationary, unless collecting

intensity data for structural refinement, so there is no need for the sophisticated goniometers required in other micro-crystallography techniques. It follows that data collection may be extremely fast (orders of magnitude faster than monochromatic data collection) and samples may be very small. These two characteristics permit ultrafast time or space resolved studies of single crystals. Many synchrotrons have one or more beamlines dedicated to the Laue method (Lennie et al. 2007; Nozawa et al. 2007; Budai et al. 2008; Tamura et al. 2009).

The Laue method has several interesting applications in geoscience. It is possible to efficiently collect accurate maps of the crystallites size, morphology and mutual orientation of the grain distribution in a rock sample in one, two or three dimensions (Ishida et al. 2003; Courtin-Nomade et al. 2008, 2010; Wenk et al. 2011), or to study the residual stress and orientation of the stress tensor in crystals embedded in rocks (Kunz et al. 2009; Chen et al. 2011a,b). In these studies, the lattice parameters are known beforehand with good approximation simplifying the indexing of the Laue pattern. Compared to electron back scattering techniques, mapping of crystal orientation and lattice strain may be determined with greater accuracy and with depth resolution in a non-destructive fashion. The Laue method is also useful for the characterization of micro-minerals embedded in rocks (Kariuki and Harding 1995), this is particularly valuable for extraterrestrial and rare specimens. Laue maps may be overlapped with compositional or spectroscopic maps. By using a beam of less than 2 μm, Ivanov et al. (2000) characterized the structure of florenskyite, FeTiP, a new phosphide mineral embedded in a meteorite thin section. Shock waves can be used to produce conditions of planetary interiors on small samples for a very short time; the *in situ* characterization of these materials must be ultrafast and if the specimen is a single crystal monochromatic diffraction cannot be performed. Laue exposures have been used to characterize crystals under shock compression with a resolution of nanoseconds in pump-and-probe manner (Ichiyanagia et al. 2007; Suggit et al. 2010).

Powder diffraction

Introduction. X-ray powder diffraction is a crystallographic technique for characterizing structure and phase composition of crystalline samples when the sample is prepared in a polycrystalline form. Powder diffraction is one of the principal research tools of mineralogists, since many minerals are available in polycrystalline form. There is a number of very good books and monographs offering a comprehensive and detailed overview of modern powder diffraction, in particular Bish and Post (1989), Pecharsky and Zavalij (2009) and Dinnebier and Billinge (2008) can be recommended to a reader who would like to develop a more in-depth understanding of the experimental aspects and theory.

The principal condition which needs to be fulfilled to assure sufficient quality of experimental powder diffraction results is satisfactory ***particle statistics***. Powder diffraction experiments typically require as many as 10^6 micrograins of the sample in the X-ray illuminated volume, with random/uniform distribution of grain orientations.

In single crystal experiments with monochromatic radiation, the crystal needs to be re-oriented for each diffraction event. However, in the case of powder diffraction, if the particle statistics conditions are satisfied, then there are grains that are randomly oriented into all the many diffracting conditions, and therefore diffraction from all of the lattice plane families is observed simultaneously. Another consequence of powder particle statistics is the shape of the diffracted signal. In single crystal diffraction, once diffraction condition is met, a directional beam is scattered from the sample along vector $\vec{S}_d^{hkl}$, which can be calculated from the Ewald construction:

$$\vec{S}_d^{hkl} = \vec{S}_0 + \lambda \breve{R} \vec{r}_{hkl} \tag{12}$$

where $\vec{S}_0$ is incident beam vector, $\vec{S}_d^{hkl}$ is diffracted beam vector, $\vec{r}_{hkl}$ is the scattering vector, and $\breve{R}$ is goniometer rotation matrix.

With powder samples, the different grains that are aligned for scattering of a specific diffraction peak have many possible azimuthal orientations around the beam, and the diffracted signal assumes a conical shape (*Debye-Scherrer cone*) centered around the incident beam direction.

Powder diffraction performed with a polychromatic incident beam leads to a continuous diffraction signal with smooth intensity variations as a function of angle and no distinct spatially resolved peaks. Such signal can only be interpreted if an energy-resolving detector is used.

Powder diffraction measurement. A goal of the typical powder diffraction experiment is to measure the angles and intensities of observable diffraction peaks. A critical factor determining the quality of diffraction data is the resolution, measured as $\Delta d/d$, where d is the d-spacing, and Δd its uncertainty. For high resolution synchrotron powder instruments $\Delta d/d$ is often in the 10^{-4} range. High resolution (i.e., low value of $\Delta d/d$) means that peak positions are more accurately determined, and peaks at similar d-spacing values can be better resolved.

Depending on the type of incident radiation used, the powder diffraction experiment can be carried out with a polychromatic beam in energy-dispersive mode (EDX) (using a solid state detector with energy resolution) or with monochromatic radiation in angular dispersive mode (ADX).

Energy dispersive method. The EDX experiment has the advantage of a stationary point detector, which does not require much angular access to the sample. The detector is placed at some fixed scattering angle (typically near 10°). This feature is particularly useful in experiments with sophisticated sample enclosures such as Large Volume Presses, or Diamond Anvil Cells, which significantly obscure access to the sample (Baublitz et al. 1981). The signal in the solid state detector is acquired as intensity vs. energy of the diffracted photons. The simultaneous accumulation of the signal over a wide range of energies (usually 5-100 keV) makes the EDX data acquisition quite fast. The energy scale of the detector is usually calibrated using a set of radioactive sources with known values of emission energies. Accurate calibration of the detector angle is performed with a diffraction standard. The main disadvantage of the polychromatic approach is the limited-energy resolution of the available detectors. Typical Ge-based solid state detectors have a resolution of about 25 eV. The uncertainty in the diffraction peak energy measurement translates into uncertainty in the d-spacing determination as follows:

$$\frac{\Delta d}{d} = \frac{1}{d}\left|\frac{\partial d}{\partial \lambda}\right|\Delta\lambda + \frac{1}{d}\left|\frac{\partial d}{\partial \theta}\right|\Delta\theta = \frac{\Delta E}{E} + \left|\cot\theta\right|\Delta\theta \qquad (13)$$

As a consequence of the limited energy resolution, EDX diffraction peaks are typically quite broad and for more complex or lower symmetry crystal structures resolving peak overlaps at higher energies becomes a significant problem. The EDX method was widely used in the 1980s and 1990s but has become much less popular with the introduction of area detectors for monochromatic experiments. In principle, it is possible to use peak intensities recorded in the EDX experiment for structure refinement, however, complicated energy-dependent corrections (e.g., incident intensity, detector quantum efficiency, sample and sample environment absorption, etc.) need to be applied (Yamanaka and Ogata 1991; Neuling et al. 1992). Recently, an interesting hybrid modification of the EDX method, named Combined Angle- and Energy-dispersive Structural Analysis and Refinement (CAESAR) has been proposed (Wang et al. 2004), which greatly enhances the resolution of the diffraction data while still taking advantage of the energy-dispersive detector. However, the data collection process in CAESAR is several orders of magnitude more time consuming, compared to the classical EDX.

Monochromatic method. Two principal ways to detect the diffraction signal scattered from the sample in the ADX experiment are either to use a scanning point-detector (e.g.,

scintillator-based), which measures scattered intensity as a function of scattering angle along a single direction at a time, or to use an imaging area detector which can be placed in the diffracted signal path and intersects the diffraction cones. Each of these two approaches has its benefits and disadvantages and we will briefly review specific applications for which one is recommended over the other.

High resolution powder instruments. When using monochromatic incident X-rays in the ADX experiment, the spectral purity of both the incident, as well as scattered radiation contributes to the error in the *d*-spacing determination through the ΔE term in Equation (13). High resolution instruments feature sophisticated monochromators composed of several highest-quality single crystals (typically Si), which remove most of the unwanted energy-components of the incident beam. The diffraction signal often contains additional energy contributions that arise from Compton scattering, X-ray fluorescence, thermal diffuse scattering, *etc.* To filter out these contributions, high resolution instruments are often equipped with an additional detector-path monochromator (analyzer) which provides energy-filtering.

The most popular instrument geometry for high resolution powder diffraction is Bragg-Brentano design, shown in Figure 7, in which the incident beam, defined by a set of slits, diverges from a small source towards the sample, and then the diffraction signal, scattered from the sample, converges (again defined by a set of slits) towards the point detector. To keep the incident and diffracted beam path symmetric, a $\theta/2\theta$ rotation is typically used, in which during the scanning process the sample is rotated by θ, while the detector moves by 2θ with each step. Modern synchrotron-based high resolution instruments are equipped with multiple analyzer-detector banks which permit simultaneous data collection in several 2θ ranges at the same time and significantly shorten the data collection time (Wang et al. 2008). Figure 8 shows a comparison of instrumental function (angle-dependence of peak width for a peak profile standard) for a high resolution instrument and an instrument employing an area detector.

Powder experiments with area detectors. The two most common types of area detectors used for X-ray diffraction include charge coupled devices (CCDs) and image plate (IP)

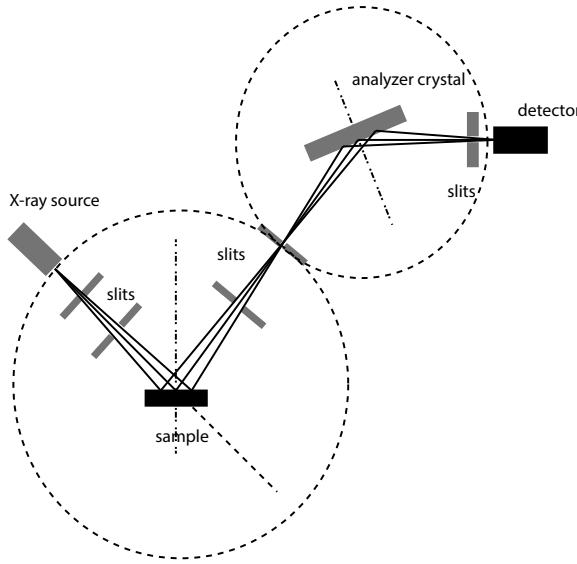

Figure 7. Bragg-Brentano high resolution diffractometer with analyzer crystal.

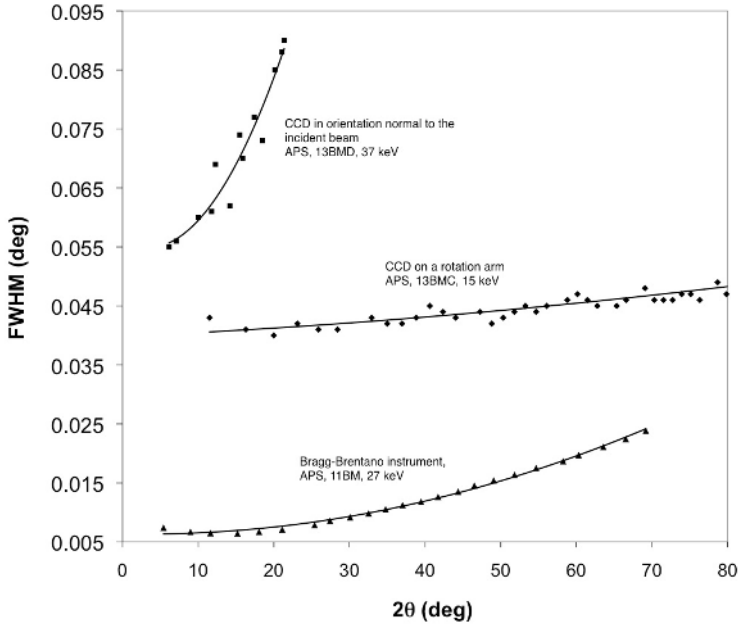

Figure 8. Comparison of instrumental function for a high-resolution instrument and an instrument employing an area detector.

detectors. Burns (1998) presented an overview of many applications of CCD detectors in the X-ray diffraction analysis of minerals. CCDs utilize a phosphor screen which converts diffracted X-rays into visible light and then use electronic chip of the type used in digital photographic cameras to detect the visible light image. IP detectors store the diffraction information by utilizing the activation of Eu^{2+} centers present on the surface of the plate. The signal can then be read with the use of photo-stimulated luminescence in a scanner. CCD detectors are characterized by much shorter readout time (few seconds) than IPs with on-line scanners (few minutes), but have higher background noise and smaller dynamic range.

From the point of view of imperfect particle statistics, the area detector has the advantage of sampling multiple points of intersection of the diffraction cone with the detector surface. If significant non-uniformity of the intensity of diffracted signal occurs as a function of azimuth (along the ring of intersection of Debye-Scherrer cone with the detector surface), then area detectors can be used to average the intensity and better model the intensity distribution. A scanning point-detector, on the other hand, intersects the Debye-Scherrer cone only at one point, and therefore is highly susceptible to the effects of preferred orientation, which may result in peak intensity measurement significantly departing from the theoretical structure factor amplitudes. These effects can be accounted for by including a preferred orientation model in the refinement of the structure, but this always significantly reduces the reliability of the structure determination.

Because of the relatively small size of the CCD chips, CCD detectors often use optical taper, which de-magnifies the image created on the phosphor to match the size of the chip. This permits a large active area of detection and increases angular coverage for single exposure. The taper, however, may introduce an optical distortion to the image and a special distortion correction is typically required, which can be calibrated. Most modern CCD detectors apply spatial correction immediately after the diffraction pattern is taken, and the bitmap image that

is saved is already spatially corrected. Another correction needed for CCD detectors is a dark current correction, which accounts for the electronic noise contribution.

Area detectors need to be calibrated prior to use for powder data collection. The calibration procedure determines the sample-to-detector distance, point of intersection of the incident beam with the detector surface, as well as the detector orientation with respect to the incident beam. The incident energy is usually calibrated independently of the detector calibration, e.g., using an absorption edge of a metal foil. The detector calibration is carried out with a diffraction standard such as LaB_6, CeO_2 or Si powder. Once a detector calibration is constrained, it can be used to integrate a diffraction image into a one-dimensional pattern of $I(2\theta)$.

Popular computer programs that can be used to calibrate detector geometry and integrate diffraction images include Fit2d (Hammersley et al. 1996), Two2One (Vogel et al. 2002; Vogel and Knorr 2005), Powder3d and Powder3d_IP (Hinrichsen et al. 2006) and Datasqueeze (Heiney 2005).

A very comprehensive review of all aspects of the use of area detector for X-ray diffraction applications can be found in He (2009).

Peak intensity. In the powder diffraction technique, the peak intensity is derived from the crystal structure through the structure factor equation in much the same way as in single-crystal diffraction. The formula for the calculation of the overall intensity contribution of one phase p to the diffraction pattern has the following form:

$$I_p^i = S_F \frac{\lambda^3 f_p}{V_p^2} \sum_{hkl} \left(m_{hkl} L_{hkl} P_{hkl} A_{hkl} S_{hkl}^i(\theta) \left| F_{hkl} \right|^2 \right)_p + bkg^i \tag{14}$$

where S_F is the global scale factor (applicable to all phases present in the sample, reflecting the volume of the illuminated sample, incident intensity, etc.), f_p is the volume fraction of phase p, V_p is the unit cell volume of phase p, L_{hkl} is the combined Lorenz and polarization correction, m_{hkl} is the peak multiplicity, F_{hkl} is the structure factor, $S_{hkl}^i(\theta)$ is the peak profile function, P_{hkl} is the preferred orientation correction, A_{hkl} is the absorption correction, and bkg^i is the background term.

The main difference between peak intensity in powder (Eqn. 14) and single crystal diffraction (Eqn. 5) is the peak multiplicity, m_{hkl}. In single crystal diffraction experiments, the symmetry-dependent peaks, which have exactly the same d-spacing, are observed independently, and should all have identical intensities. In powder diffraction these peaks overlap with each other and their intensities sum together. Depending on the number of symmetry equivalent peaks, different numbers of peak intensities are summed, and therefore, in order to compare powder and single-crystal peak intensities, the former have to be divided by the peak multiplicity factor.

The types of intensity corrections that have to be applied to powder diffraction data prior to structure analysis (L_{hkl}, P_{hkl}, and A_{hkl}) are analogous to corrections used in single crystal diffraction.

Peak overlap. One of the principal challenges of powder diffraction is the one-dimensional character of the diffraction data and resulting peak overlap. Since all of the Debye-Scherrer cones are simultaneously observed and all have the same geometric shape, the cones corresponding to reciprocal vectors with the same, or very close, d-spacings overlap with each other. If two or more peaks are too close to each other it becomes difficult to reliably fit their positions and relative intensities (both of which are necessary for unit cell and crystal structure refinement). The peak width and the "density" of peaks increase at higher scattering angles, and the problem becomes much more pronounced in this region. Peak overlap is particularly dramatic for low symmetry structures, in which many closely spaced peaks occur throughout

the whole powder pattern. Problems with excessive peak overlap can be at least partially resolved with the use of high resolution powder diffraction instruments, which contribute very little instrument-related broadening to the experimental data. For experiments with broader peaks and significant peak overlap, refinement methods which constrain the peak positions from the unit cell (LeBail, Pawley and Rietveld methods) provide some help, as peak positions and intensities are not individually and independently refined, however, the problem with reliably constraining the intensity partitioning remains.

Peak width. In powder diffraction experiments the observed peak width is a convolution of sample-related effects and instrument-related effects. Decoupling these two classes of effects from each other permits the understanding of potentially important sample characteristics.

Typical instrument-related factors, which affect observed peak width, include divergence of the incident beam, spectral purity (energy-width) for monochromatic beams, detector acceptance angle (for point detectors) and diffracted signal incidence angle on the detector (for area detectors). In general, peak width effects of the instrument vary as a function of scattering angle in a regular way. One of the possible equations to account for this factor, which was originally derived for neutron diffraction and Gaussian peak shapes, is known as the Caglioti law (Caglioti et al. 1958):

$$H_{hkl}^2 = U\tan^2\theta_{hkl} + V\tan\theta_{hkl} + W \tag{15}$$

where H_{hkl} is full width at half maximum of the given peak, and U, V and W parameters can be calculated according to specification of a particular instrument and source, but are usually refined. Caglioti's law was later generalized for application to synchrotron and laboratory X-ray instruments (Sabine 1987; Gozzo et al. 2006).

Scherrer (1918) first observed an empirical rule that the integral breadth of the diffraction peak, β_{hkl} defined as the ratio of peak area to peak maximum, is proportional to the average particle size of the sample D:

$$\beta_{hkl} = \frac{\lambda K_\beta}{D\cos\theta_{hkl}} \tag{16}$$

where K_β is a dimensionless particle shape factor, with a typical value of about 0.9, which varies with the actual shape of the crystallites. The Scherrer formula is useful for characterizing statistical distributions of grain sizes in nanoparticle materials. It has to be emphasized that the Scherrer formula is not applicable to grains larger than about 0.1 μm, which precludes those observed in most metallographic and ceramic microstructures.

Besides the particle size, the diffraction peak width is also affected by the statistical distribution of the unit cell parameters (strain) of individual micrograins. Real materials often exhibit defects, which affect the micrograin unit cell parameters. Fluctuations of these individual unit cell parameters, in turn, affect position, size and shape of powder peak profiles. In general, two types of strain are considered in relation to powders: macrostrain (macroscopic homogeneous strain affecting all grains equally), and microstrain (non-homogenous strain field - on the length scale of individual crystallites, which can significantly vary from grain to grain). Macrostrain affects mainly peak positions, while microstrain results in peak width changes. Stokes and Wilson proposed a simple relation for the estimation of the effect of strain on peak profiles:

$$\beta = 2\left\langle \varepsilon^2 \right\rangle^{\frac{1}{2}} \tan\theta \tag{17}$$

where ε is the lattice strain. By combining the size and strain contributions, the following relation, originally proposed by Williamson and Hall (1953) is obtained:

$$\cos\theta_{hkl} = \frac{\lambda K_\beta}{\beta_{hkl} D} + \frac{2\left\langle \varepsilon^2 \right\rangle^{\frac{1}{2}}}{\beta_{hkl}} \sin\theta \tag{18}$$

If peak breadths are plotted in $y = \beta\cos\theta$, $x = \sin\theta$ coordinate system, then a linear regression can approximate the average grain size from the line intercept, and the average microstrain from the line slope. It should be noted that Equation (18) does not account for instrumental broadening, therefore instrumental function should be calibrated with a line profile standard (e.g., LaB_6 supplied by the National Institutes for Standards in Technology) and subtracted from the observed peak breadths prior to the Williamson-Hall analysis.

While very useful for semi-quantitative interpretation of grain size and strain effects, the Williamson-Hall method is very approximate. Methods based on Fourier analysis and convolution decomposition are recommended when more quantitative results are required (e.g., Warren-Averbach method; Warren 1969).

Preferred orientation. With perfect particle statistics the distribution of scattered intensity around the diffraction cone should be uniform, except for the incident radiation polarization effects. In many real cases, however, the requirement for random distribution of micrograins in the powder sample cannot be satisfied e.g., because of highly anisotropic grain shapes, or stress-history. Departure from a uniform distribution of grain orientations is known as ***preferred orientation***. For example metallurgical samples are essentially polycrystalline powders with frozen grain orientations. The processes involved in fabrication of the metal (e.g., rolling, drawing, casting) leave a specific record of preferred orientation pattern, which can often be traced back to the manufacturing methods using diffraction data. Extensive review of all aspects of texture and preferred orientation can be found in Kocks et al. (1998).

The two most popular methods for the inclusion of the effect of preferred orientation in structure refinement from powder data are the Dollawse-March model (March 1932; Dollase 1986) and the spherical harmonics approach (Bunge 1965; Roe 1965). In the Dollase-March method, the P_{hkl} correction in Equation (14) is calculated according to the following formula:

$$P = \frac{1}{m} \sum_n \left(P_{MD}^2 \cos^2 \alpha_n + \frac{\sin^2 \alpha_n}{P_{MD}} \right)^{-\frac{3}{2}} \tag{19}$$

where summation is over the equivalent peaks occurring at the same *d*-spacing, *m* is the multiplicity factor, α_n is the angle between the reciprocal vector corresponding to the n-*th* peak and the vector of preferred orientation, and P_{MD} is the additional parameter included in the refinement which accounts for the degree of preferred orientation.

Results of preferred orientation modeling are often represented in a form of graphs, known as ***pole figures*****,** showing the probability of finding certain crystallographic directions of polycrystalline grains along different directions in the sample.

Peak and whole pattern fitting

Individual peak fitting. The simplest approach to retrieving diffraction peak position and intensity information from experimental powder pattern is to perform peak fitting with appropriate peak shape function for each peak individually. Typical profile functions used in powder diffraction analysis include:

Gaussian:

$$S_{hkl}(2\theta) = G(2\theta) = I_h \exp\left(-0.6931 K \left(2\theta - 2\theta_{hkl} \right)^2 \right) \tag{20}$$

Lorenzian:

$$S_{hkl}(2\theta) = L(2\theta) = I_h\left[1 + K\left(2\theta - 2\theta_{hkl}\right)^2\right]^{-1} \quad (21)$$

Pseudo-Voigt

$$S_{hkl}(2\theta) = I_h\left[aL(2\theta) + (1-a)G(2\theta)\right] \quad (22)$$

and Pearson-VII:

$$S_{hkl}(2\theta) = I_h\left[1 + 2^{1/M}K(2\theta - 2\theta_{hkl})^2\right]^{-M} \quad (23)$$

where $K = 4(1 + S)/H^2$, I_h is peak height, H is FWHM, S is the asymmetry parameter, and M is additional exponent parameter used in the Pearson-VII function. In individual peak refinement, the peak position θ_{hkl} is usually one of the directly refined parameters, and integrated peak intensity is calculated from other refined parameters (intensity at peak maximum, peak width, peak asymmetry parameters, etc.) using analytical formulas for the particular peak shape function used. In this approach, peak positions are not constrained in any way and the unit cell is calculated using least squares optimization, after assigning each of the fitted peaks appropriate Miller indices. Integrated peak intensities obtained from individual peak fitting can, in principle, be used for structure refinement in the same way as single crystal intensities. A free computer program that can be used to perform individual peak fitting is CrystalSleuth (Laetsch and Downs 2006).

A popular computer program which can be used to refine unit cell parameters from fitted peak positions with assigned indices is Unitcell (Holland and Redfern 1997). Unitcell implements several possible statistical weight models that can be assigned to each peak, as well as an algorithm which identifies outliers that do not follow general statistical trends (e.g., because of errors in fitting closely overlapping peaks).

Individual peak fitting is an acceptable approach for very simple crystal structures with high symmetry, in which peak overlap is not significant. For more complex crystal structures and lower symmetry cases peak overlap, particularly at high scattering angles, makes fitting of individual profiles for groups of closely spaced peaks problematic.

One case in which individual peak fitting may have advantages over other fitting approaches are experiments with significant nonhydrostatic stress. In such cases, the individual powder peaks may move at a different rate as a function of stress, depending on the linear modulus along the appropriate lattice direction. The fact that the peak positions are not constrained in any way during the refinement accounts for this effect. It should be noted that it is possible to implement a microstrain model into Rietveld refinement (Daymond et al. 1997, 1999), however this approach introduces additional fitting parameters and is quite sophisticated and, as a result, not used very often.

Rietveld refinement. The ultimate tool for structure refinement from powder diffraction data is Rietveld refinement (Rietveld 1967, 1969). Conceptually, the idea of Rietveld refinement is very simple. The observed diffraction pattern I_i^{obs} (index i corresponds numbers all measured spectral points) is assumed to be a sum of background function bkg_i and contributions from all individual diffraction peaks $I_{i,k}^{obs}$

$$I_i^{obs} = bkg_i + \sum_k I_{i,k}^{obs} \quad (24)$$

where index k refers to individual diffraction peaks. $I_{i,k}^{obs}$ includes appropriate peak profile functions. Once individual observed peak intensities $I_{i,k}^{obs}$ are extracted, they can be compared with calculated peak intensities $I_{i,k}^{calc}$, obtained from the approximate crystal structure model. The refinement involves minimization of a weighted sum of squares WSS, defined as follows:

$$WSS = \sum_k w_k \left(I_k^{obs} - I_k^{calc} \right)^2 \qquad (25)$$

$$w_k = \frac{1}{I_k^{obs}}$$

while varying the structural parameters (unit cell parameters, fractional atomic coordinates, atomic displacement parameters, site occupancy factors) as well as the peak profile and background functions to achieve the best match between the observed and calculated pattern. In the original papers (Rietveld 1967, 1969) which introduced the method, the background was modeled prior to structure refinement, so that the minimization was done with a background-subtracted pattern, and the statistical weights were uniform. In the modern implementation of the method, the background is fit at the same time as the structure is determined.

The main difference between the Rietveld approach and single-crystal refinement is that all the additional parameters need to be refined at the same time as the structural parameters, while the number of independent observations is typically much lower than in single-crystal case. Due of this deficiency, optimization of all of the refinable parameters at the same time can lead to divergence and unrealistic values of the parameters. As a consequence, Rietveld refinement is usually carried out in stages in which different classes of parameters are included in the optimization individually, while other parameters are fixed. Since Rietveld and Le Bail refinement include the same definition of peak profile functions and their angular dependence, it is a common practice to first carry out a Le Bail refinement to optimize unit cell parameters, peak profiles, and background function independent of the structure, and then use these as starting values for a Rietveld refinement in which peak intensities are derived from the structure. Because of the overparametrization problem Rietveld refinement is usually carried out with isotropic atomic displacement parameters, and often includes constraints or restraints based on crystallochemical assumptions.

A review of the principles and examples of Rietveld analysis is presented by Von Dreele in Dinnebier and Billinge (2008). For a more in-depth introduction to the method, Bish and Post (1989) as well as Young (1993) are recommended.

Most popular computer programs which can be used to carry out Rietveld refinement include GSAS (Larson and Von Dreele 2000; Toby 2001), Fullprof (Rodriguez-Carvajal 1990), Rietan (Young 1993) and MAUD (Lutterotti et al. 1999).

Pawley and Le Bail whole pattern refinement. Because of the problems with individual fitting of closely overlapping peak it is difficult to use that approach to extract reliable peak intensities that could be used for solution of unknown crystal structures. To resolve this situation, in the 1980's, a new whole pattern refinement method, which constrains peak positions to values determined by unit cell parameters, while allowing individual peak intensities to be refined independently, was introduced (LeBail et al. 1988; Pawley 1981). This new approach dramatically reduces the number of refined parameters (for N observed peaks instead of refining N peak position one uses 6 or less cell parameters) and aids in more reliable refinement of intensity partitioning between closely overlapping peaks. In the Pawley method (Pawley 1981) peak profile width is constrained by the Caglioti law with the three refinable parameters U, V, W as defined in Equation (15).

Constraints are introduced to help provide stability of the refinement of closely overlapped peaks. The Pawley method also calculates a co-variance matrix describing how the extracted peak intensities correlate with each other and provides reasonable estimates of peak intensity standard deviations. The disadvantage of the Pawley method is that the inclusion of all the peak intensities as independent parameters in the optimization creates a challenging numerical

problem for computer software (very large matrix that has to be inverted) and results in long computation times.

To solve this numerical challenge a different approach for determining peak intensities, but still taking advantage of constrained peak positions from unit cell parameters was introduced by Le Bail et al. (1998). The Le Bail method uses a two-step iterative process in which peak intensities are no longer treated as refinable parameters. As a consequence, the least-squares matrix is much smaller and the optimization significantly faster than in the Pawley approach. In Rietveld refinement, the partitioning of calculated intensity I_i^{calc} between overlapping peaks $I_{i,k}^{calc}$ is determined by the structure model. In order to obtain observed intensities for the same peaks, it is then assumed that the I_i^{obs} partitions in the same way as I_i^{calc}. The caveat of this approach is that for overlapping peaks, an inaccurate or wrong model will lead to improper estimation of I_i^{obs}. Le Bail peak intensity extraction starts from a uniform partitioning of all calculated intensities $I_{i,k}^{calc} = 1$. The Rietveld algorithm is then used to extract I_i^{obs}, after which the $I_{i,k}^{calc}$ are reset from the extracted $I_{i,k}^{obs}$. This approach assures optimal estimates of peak intensities in which the intensities of completely overlapped peaks is apportioned according to peak multiplicity.

Le Bail refinement is often used to retrieve unit cell parameters and confirm the correctness of indexing in cases when the quality of peak intensities is insufficient for structure refinement or if the structure of the sample is not known.

Parametric Rietveld refinement. While Rietveld refinement is a very valuable tool for retrieving information about the atomic arrangements of the crystalline sample, the reliability of the structure models derived from Rietveld analysis often suffers from insufficient number of independent observations. In some extreme cases is has even been demonstrated that a refinement with a wrong unit cell and essentially wrong structure can yield figures of merit that look satisfactory (Buchsbaum and Schmidt 2007). This problem is particularly dramatic for experiments at nonambient conditions (e.g., high pressure or high temperature), in which the sample environment is complicated by the presence of heaters, high pressure cells, etc. that contribute unwanted signal and intensity-affecting effects to the observed pattern. On the other hand, when investigating systematic trends, a time, temperature or pressure series of diffraction patterns, all collected within the same phase stability field are not completely independent from each other (because the structure changes in a continuous way). Based on this assumption, Stinton and Evans (2007) proposed an approach to fitting all of these serial diffraction patterns at the same time while tying the refined parameters together by means of polynomial equations. This method has been demonstrated to yield much more reliable and physically reasonable structure models than individual Rietveld refinements (Bish and Howard 1988; Agostini et al. 2010; Halasz et al. 2010; Müller et al. 2011). Additional benefit of the parametric Rietveld refinement is the fact that it produces a model of the structural evolution accompanying the studied process, which can be much easier understood than a series of individual models.

Quantitative analysis of phase mixtures. The powder pattern of a crystalline substance is like its fingerprint, and, as can be seen from Equation (14), its overall intensity is dependent on the illuminated volume of the sample. For samples composed from multiple crystalline phases, each phase contribution is scaled by the volume fraction of the given phase. Powder diffraction-based quantitative analysis (QA) provides for the determination of the composition of phase mixtures by carrying out a refinement that includes phase volume fractions. The most popular type of QA analysis with powder data is carried out using multi-phase Rietveld refinement (Bish and Howard 1988).

In principle, it is possible to carry out powder diffraction based QA even if the structure of some or all of the phase mixture components are not known (e.g., in case of poorly crystalline

or amorphous phases) (Scarlett and Madsen 2006). In such cases, it is necessary to obtain pure-phase samples of each of the components and measure calibration patterns from mixtures of these pure components with an internal diffraction standard (a common internal standard is Al_2O_3 corundum), which yields information about relative total scattering power of each component. Chipera and Bish (2002) introduced software called FULLPAT for QA if a full set of such calibration data is available for all components.

The atomic pair distribution function technique (PDF)

The atomic pair distribution function technique, introduced in the 1930s for the experimental investigation of liquid and crystalline materials (Debye and Menke 1930; Warren 1934; Warren and Gingrich 1934), has found renewed interest and has been extended to materials with a wide range of ordering, from completely amorphous to nanocrystalline. The technique is useful for producing an estimate of the probability distribution of interatomic separations. A comprehensive description of the technique can be found in Egami and Billinge (2003); and summarized in several review papers (Proffen et al. 2003; Billinge 2004; Billinge and Kanatzidis 2004; Page et al. 2004; Proffen 2006). Bragg peaks and diffuse scattered radiation are treated as a whole in the PDF analysis. The formalism of the PDF technique is general; no assumptions are made on the atomic structure of materials, instead it is concerned with the frequency of occurrence of atoms as a function of interatomic distances. The data collection procedure is basically the same as for collecting a powder diffraction pattern to high Q values ($Q = 4\pi\sin\theta/\lambda$ is the magnitude of the scattering vector or momentum transfer), usually obtained using high energy synchrotron radiation (the real space resolution is inversely related to the wavelength), but also polychromatic laboratory sources (e.g., Di Marco et al. 2009). The data collection time varies from several hours to seconds depending on the detector type and the sample characteristics. Measurements are carried out to high-Q values in order to avoid artificial ripples from the Fourier transformation termination. Particular care must be taken in the measurement of the background which is subtracted from the sample data; inaccurate background subtraction can produce severe artifacts in the analysis because the full pattern is used to constrain structural parameters. From the experimental coherent intensities I(Q), expressed as a function of the momentum transfer Q, the total scattering structure function is calculated:

$$S(Q) = \frac{I(Q) - \sum c_i \left| f_i(Q) \right|^2}{\left| \sum c_i f_i(Q) \right|^2} \tag{26}$$

where c_i and f_i are the respective atom concentrations and atomic scattering factors of the i^{th} atoms, summed over the scattering volume. The experimental PDF is denoted with the function $G(r)$, calculated as the Fourier transform of the total scattering:

$$G(r) = 4\pi r\left[\rho(r) - \rho_0\right] = \frac{2}{\pi}\int_0^{Q\max} Q\left[S(Q) - 1\right]\sin(Qr)dQ \tag{27}$$

where ρ_0 is the average atomic number density and $\rho(r)$ is the atomic pair density. Peculiar to the PDF technique is that a plot of the $G(r)$ function is a rather intuitive pattern showing real space maxima corresponding to interatomic distances "weighted" by the scattering factor of the pairs of atoms and the frequency with which they occur. Highly ordered and symmetric materials have well defined interatomic distances for many coordination shells and therefore show sharp peaks in the $G(r)$ plots, while disordered materials have a greater spread of interatomic distances and therefore they will show broad peaks, particularly at high r. Liquids, where the ordering vanishes quickly with distance and so interatomic distance randomize rapidly beyond the first coordination shell (short range ordering), show peaks confined to a fairly low-r range. The interpretation of a PDF pattern is not necessarily unique. The technique

is especially suitable for the analysis of elusive structures of complex minerals such as clays and weathering products (Gualtieri et al. 2008; Di Marco et al. 2009; Fernandez-Martinez et al. 2010; White et al. 2010) where Bragg and diffuse components are equally important. The analysis of PDF patterns is a challenging task, but can yield satisfactory results when coupled with other experiments (Krayzman et al. 2009) and first principle calculations (White et al. 2010; Fernandez- Martinez et al. 2010). The PDF technique is also a useful tool in the structural analysis of materials with long range ordering, Billinge and Kanatzidis (2004) discuss examples where incorrect structural solutions from single crystal analysis are readily verified by means of PDF analysis. Toby and Billinge (2004) present an important analysis of the statistics of structural determinations with the PDF technique. In a novel application of the technique, Li et al. (2011), studied the effect of arsenate doping in γ-alumina by analyzing the differential PDF of untreated and treated samples.

The Fernandez-Martinez et al. (2010) study of the structure of schwertmannite, $(Fe_8O_8(OH)_{8-x}(SO_4)_x$, an important scavenger of As and Se contaminants, offers an instructive example of the application of the PDF techniques. Occurring as poorly crystallized nanosize material, schwertmannite achieved the status of mineral only recently (Bigham et al. 1994) due to the difficulty in defining both its composition and structure. The modeling of the PDF pattern is performed starting from the structure of the sulfate-free akaganeite (Post et al. 2003), a mineral with an arrangement of FeO_6 octahedra similar to schwertmannite. Figure 9, with simulated partial and total PDFs of sulfate doped akaganeite, shows how single atomic pairs sum to give the total $G(r)$. Fe-Fe and Fe-O pairs provide a strong contribution to the total scattering and therefore are better resolved. Nonetheless, the short S-O bond results in a distinct feature in the simulated and experimental PDFs (Fig. 9). The authors used the intensity of the S-O and Fe-O correlations and their weighting factors to estimate the amount of sulfate in the sample. The fitting of the PDF data provides evidence of a triclinic distortion of the unit

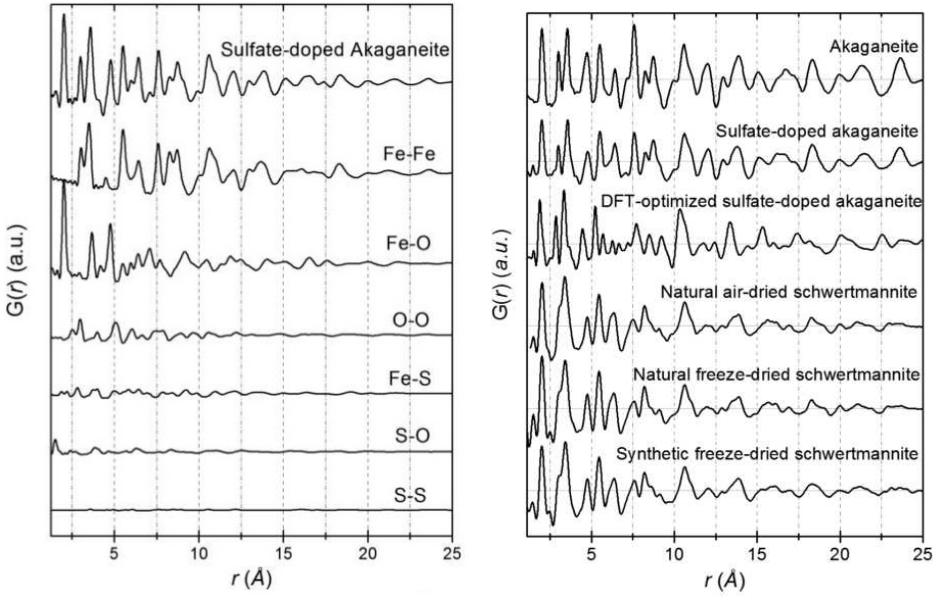

Figure 9. Simulated partial and total PDFs of sulfate-doped akaganeite (*left*) and comparison between calculated (upper three) and experimental (bottom three) PDFs of the oxyhydroxysulfates (*right*) by Fernandez-Martinez et al. (2010).

cell of schwertmannite from the monoclinic akaganeite, however it could not discriminate two different models for the arrangement of the FeO_6 octahedra.

ACKNOWLEDGMENTS

The UNLV High Pressure Science and Engineering Center (HiPSEC) is supported by DOE-NNSA Cooperative Agreement DE-FC52-06NA262740. GeoSoilEnviroCARS is supported by the National Science Foundation - Earth Sciences (EAR-0622171) and Department of Energy - Geosciences (DE-FG02-94ER14466). The APS is supported by DOE-BES, under Contract No. DE-AC02-06CH11357.

REFERENCES

Agostini G, Lamberti C, Palin L, Milanesio M, Danilina N, Xu B, Janousch M, van Bokhoven JA (2010) *In situ* XAS and XRPD parametric Rietveld refinement to understand dealumination of Y zeolite catalyst. J Am Chem Soc 132:667-678

Als-Nielsen J, McMorrow D (2011) Elements of Modern X-ray Physics. Wiley, Hoboken

Angel RJ, Downs RT, Finger LW (2000) High-temperature – high-pressure diffractometry. Rev Mineral Geochem 41:559-597

Aroyo MI, Kirov A, Capillas C, Perez-Mato JM, Wondratschek H (2006a) Bilbao crystallographic server. II. Representations of crystallographic point groups and space groups. Acta Crystallogr A 62:115-128

Aroyo MI, Perez-Mato JM, Capillas C, Kroumova E, Ivantchev S, Madariaga G, Kirov A, Wondratschek H. (2006b) Bilbao crystallographic server: I. Databases and crystallographic computing programs. Z Kristallogr 221:15-27

Baublitz MA, Arnold V, Ruoff AL (1981) Energy dispersive-X-ray diffraction from high-pressure polycrystalline specimens using synchrotron radiation. Rev Sci Instrum 52:1616-1624

Berlepsch P, Armbruster T, Brugger J, Criddle AJ, Graeser S (2003) Tripuhyite, $FeSbO_4$, revisited. Mineral Mag 67:31-46

Bigham JM, Carlson L, Murad E. Schwertmannite, a new iron oxyhydroxysulphate from Pyhasalmi, Finland, and other localities (1994) Mineral Mag 58:641-648

Billinge SJL (2004) The atomic pair distribution function: past and present. Z Kristallogr 219:117-121

Billinge SJL, Kanatzidis MG (2004) Beyond crystallography: the study of disorder, nanocrystallinity and crystallographically challenged materials with pair distribution functions. Chem Comm 7:749-760

Billinge SJL, Thorpe MF (1998) Local Structure from Diffraction. Plenum Press, New York

Bindi L, Carbone C, Cabella R, Lucchetti G (2011) Bassoite, $SrV_3O_7 \cdot 4H_2O$, a new mineral from Molinello mine, Val Graveglia, eastern Liguria, Italy. Mineral Mag 75:2677-2686

Bindi L, Steinhardt PJ, Yao N, Lu PJ (2009) Natural quasicrystals. Science 324:1306-1309

Bish DL, Howard SA (1988) Quantitative phase-analysis using the Rietveld method. J Appl Crystallogr 21:86-91

Bish DL, Post JE (eds) (1989) Modern Powder Diffraction. Reviews in Mineralogy, Volume 20. Mineralogical Society of America

Blake AJ, Clegg W (2009) Crystal structure analysis: principles and practice. Vol. 13 International Union of Crystallography book series. 2nd ed. Oxford University Press. Oxford,

Blake DF, Vaniman D, Anderson R, Bish D, Chipera S, Chemtob S, Crisp J, DesMais DJ, Downs RT, Farmer J, Gailhanou M, Ming D, Morris D, Stolper E, Sarrazin P, Treiman A, Yen A (2009) The CHEMIN mineralogical instrument on the Mars science laboratory mission. Proceedings of the 40th Lunar and Planetary Science Conference, 1484

Bochenin VI (1973) Portable X-ray diffractometer for phase analysis of materials with a radiation source on ^{55}Fe basis. Prib Tekh Eksp 5:228-230

Boisen MB Jr, Gibbs GV (1985) Mathematical Crystallography. Reviews in Mineralogy, Volume 15. Mineralogical Society of America

Britvin SN, Rudashevsky NS, Krivovichev SV, Burns PC, Polekhovsky YS (2002) Allabogdanite, $(Fe,Ni)_2P$, a new mineral from the Onello meteorite: The occurrence and crystal structure. Am Mineral 87:1245-1249

Brown GE Jr, Sutton SR, Calas G (2006a) User facilities around the world. Elements 2:9-14

Brown PJ, Fox AG, Maslen EN, O'Keefe MA, Willis BTM (2006b) Intensity of diffracted intensities. *In*: International Tables for Crystallography. Volume C. Prince E (ed) John Wiley & Sons, Ltd, p 554-595

Buchsbaum C, Schmidt MU (2007) Rietveld refinement of a wrong crystal structure. Acta Crystallogr B 63:926-932

Budai JD, Liu W, Tischler JZ, Pan ZW, Norton DP, Larson BC, Yang W, Ice GE (2008) Polychromatic X-ray micro- and nanodiffraction for spatially-resolved structural studies. Thin Solid Films 516:8013-8021

Bunge HJ (1965) Zur darstellung allgemeiner texturen. Z Metallkd 56:872-874

Burla MC, Caliandro R, Camalli M, B Carrozzini B, GL Cascarano GL, Giacovazzo C, Mallamo M, Mazzone A, Polidori G, Spagna R (2012) SIR2011: a new package for crystal structure determination and refinement. J Appl Crystallogr 45:357-361

Burns PC (1998) CCD area detectors of X-rays applied to the analysis of mineral structures. Can Mineral 36:847-853

Caglioti G, Paoletti A, Ricci FP (1958) Choice of collimators for a crystal spectrometer for neutron diffraction. Nucl Instrum Methods 3:223-228

Chantler CT (2000) Detailed tabulation of atomic form factors, photoelectric absorption and scattering cross section, and mass attenuation coefficients in the vicinity of absorption edges in the soft X-ray (Z=30-36, Z=60-89, E=0.1 keV-10 kev), addressing convergence issues of earlier work. J Phys Chem Ref Data 29:597-1048

Chen K, Kunz M, Tamura N, Wenk H-R (2011a) Evidence for high stress in quartz from the impact site of Vredefort, South Africa. Eur J Mineral 23:169-178

Chen K, Kunz M, Tamura N, Wenk H-R (2011b) Deformation twinning and residual stress in calcite studied with synchrotron polychromatic X-ray microdiffraction. Phys Chem Mineral 38:491-500

Chichagov AV, Varlamov DA, Dilanyan RA, Dokina TN, Drozhzhina NA, Samokhvalova OL, Ushakovskaya TV (2001) MINCRYST: a crystallographic database for minerals, local and network (www) versions. Crystallogr Rep+ 46:876-879

Chipera SJ, Bish DL (2002) FULLPAT: a full-pattern quantitative analysis program for X-ray powder diffraction using measured and calculated patterns. J Appl Crystallogr 35:744-749

Clegg W (2001) Crystal Structure Analysis: Principles and Practice. Volume 6. International Union of Crystallography

Courtin-Nomade A, Vanaecker M, Kunz M, Tamura N (2008) Coupling micro-Raman and microscanning X-ray diffraction to characterize heterogeneous material. Geochim Cosmochim Acta 72:A185-A185

Courtin-Nomade A, Bril H, Beny J-M, Kunz M, Tamura N (2010) Sulfide oxidation observed using micro-Raman spectroscopy and micro-X-ray diffraction: The importance of water/rock ratios and pH conditions. Am Mineral 95:582-591

Dauter Z, Wilson KS (2007) Principles of monochromatic data collection. *In:* International Tables for Crystallography, Volume F. International Union of Crystallography, p 177-195

Davis MF, Groter C, Kay HF (1968) On choosing off-line automatic X-ray diffractometers. J Appl Crystallogr 1:209-217

Daymond MR, Bourke MAM, Von Dreele RB, Clausen B, Lorentzen T (1997) Use of Rietveld refinement for elastic macrostrain determination and for evaluation of plastic strain history from diffraction spectra. J Appl Phys 82:1554-1562

Daymond MR, Bourke MAM, Von Dreele RB (1999) Use of Rietveld refinement to fit a hexagonal crystal structure in the presence of elastic and plastic anisotropy. J Appl Phys 85:739-747

Debye P, Menke H (1930) The determination of the inner structure of liquids by X-ray means. Phys Z 31:797-798

Di Marco M, Ballirano P, Port M, Piscopiello E, Couvreur P, Dubernet C, and Sadun C (2009). Atomic pair distribution function (PDF) study of iron oxide nanoparticles in aqueous suspension. J Mat Chem 19:6354-6360

Dinnebier RE, Billinge SJL (2008) Powder Diffraction: Theory and Practice. Royal Society of Chemistry, Cambridge

Dollase WA (1986) Correction of intensities for preferred orientation in powder diffractometry - application of the March model. J Appl Crystallogr 19:267-272

Downs RT (2000) Analysis of harmonic displacement factors. Rev Mineral Geochem 41:61-87

Downs RT, Hall-Wallace M (2003) The American Mineralogist crystal structure database. Am Mineral 88:247-250

Egami T, Billinge SJL (2003) Underneath the Bragg-peaks: Structural Analysis of Complex Material. Elsevier Sci LTD, New York

Ewald PP (1921) The "reciprocal lattice" in structure theory. Z Kristallogr 56:129-156

Fernandez-Martinez A, Timon V, Roman-Ross G, Cuello GJ, Daniels JE, Ayora C (2010) The structure of schwertmannite, a nanocrystalline iron oxyhydroxysulfate. Am Mineral 95:1312-1322

Frey F, Boysen H, Jagodzinski H (2010) Disorder diffuse scattering of X-rays and neutrons. *In*: International Tables for Crystallography B. John Wiley & Sons, Ltd, p 492-539

Friedrich W, Knipping P, Laue M (1912). Sitzungsberichte der mathematisch-physikalischen klasse der koeniglich bayerischen akademie der wissenschaften zu muenchen. Proc Bavarian Acad Sci 303-322

Giacovazzo C (2011) Fundamentals of Crystallography. Oxford University Press, Oxford

Glusker JP, Trueblood KN (2010) Crystal Structure Analysis: A Primer. Oxford University Press, Oxford

Gozzo F, De Caro L, Giannini C, Guagliardi A, Schmitt B, Prodi A (2006) The instrumental resolution function of synchrotron radiation powder diffractometers in the presence of focusing optics. J Appl Crystallogr 39:347-357

Gražulis S, Daškevič A, Merkys A, Chateigner D, Lutterotti L, Quirós M, Serebryanaya NR, Moeck P, Downs RT, Le Bail A (2012) Crystallography Open Database (COD): an open-access collection of crystal structures and platforms for world-wide collaboration. Nucleic Acids Res 40:D420-D427

Gualtieri AF, Ferrari S, Leoni M, Grathoff G, Hugo R, Shatnawi M, Paglia G, Billinge S (2008) Structural characterization of the clay mineral illite-1M. J Appl Crystallogr 41:402-415

Halasz I, Dinnebier RE, Angel R (2010) Parametric Rietveld refinement for the evaluation of powder diffraction patterns collected as a function of pressure. J Appl Crystallogr 43:504-510

Hammersley AP, Svensson SO, Hanfland M, Fitch AN, Hausermann D (1996) Two-dimensional detector software: From real detector to idealised image or two-theta scan. High Pressure Res 14:235-248

Hansford GM (2011) Optimization of a simple X-ray diffraction instrument for portable and planetary applications. Nucl Instrum Meth 632:81-88

Hazen RM, Finger LW (1982) Comparative Crystal Chemistry: Temperature, Pressure, Composition, and the Variation of Crystal Structure. Wiley, New York

He BB (2009) Two-Dimensional X-ray Diffraction. Wiley, Hoboken, N.J.

Heiney PA (2005) Datasqueeze: A software tool for powder and small-angle X-ray diffraction analysis. Newsletter of the IUCr Commission on Powder Diffraction 32:9-11

Hinrichsen B, Dinnebier RE, Jansen M (2006) Powder3D: An easy to use program for data reduction and graphical presentation of large numbers of powder diffraction patterns. Z Kristallogr Suppl 23:231-236

Hochella MF Jr, Lower SK, Maurice PA, Penn RL, Sahai N, Sparks, DL Twining BS (2008) Nanominerals, mineral nanoparticles, and Earth systems. Science 319:1631-1635

Holland TJB, Redfern SAT (1997) UNITCELL: A nonlinear least-squares program for cell-parameter refinement and implementing regression and deletion diagnostics. J Appl Crystallogr 30:84

Hubbell JH, Seltzer SM (2004) Tables of X-ray mass attenuation coefficients and mass energy- absorption coefficients (version 1.4). National Institute of Standards and Technology, Gaithersburg, MD, http://physics.nist.gov/xaamdi

Ichiyanagia K, Adachi S-I, Nozawa S, Hironaka Y, Nakamura KG, Sato T, Tomita A, Koshihara S-Y (2007) Shock-induced lattice deformation of CdS single crystal by nanosecond time-resolved Laue diffraction. Appl Phys Lett 91:231918

International Tables for Crystallography (2006) 1st online ed. International Union of Crystallography. http://onlinelibrary.wiley.com/book/10.1107/97809553602060000001

Ishida H, Ogasawara Y, K Ohsumi K, Saito A (2003) Two stage growth of microdiamond in UHP dolomite marble from Kokchetav massif, Kazakhstan. J Metamorphic Geol 21:515-522

Ivanov AV, Zolensky ME, Saito A, Ohsumi K, Yang SV, Kononkova NN, Mikouchi T (2000) Florenskyite FeTiP, a new phosphide from the Kaidun meteorite. Am Mineral 85:1082-1086

Kahn R, Fourme R, Gadet A, Janin J, Dumas C, AndreE D (1982) Macromolecular crystallography with synchrotron radiation - photographic data-collection and polarization correction. J Appl Crystallogr 15:330-337

Kariuki BM, Harding MM (1995) Application of synchrotron-radiation Laue diffraction to small single-crystals of a mineral - structure determination and identification. J Synchrotron Radiat 2:185-189

King HE, Finger LW (1979) Diffracted beam crystal centering and its application to high-pressure crystallography. J Appl Crystallogr 12:374-378

Kocks UF, Tomé CN, Wenk H-R (1998) Texture and Anisotropy: Preferred Orientations in Polycrystals and Their Effect on Materials Properties. Cambridge University Press, Cambridge, UK

Krayzman V, Levin I, Woicik JC, Proffen T, Vanderah TA, Tucker MG (2009). A combined fit of total scattering and extended X-ray absorption fine structure data for local-structure determination in crystalline materials. J Appl Crystallogr 42:867-877

Kunz M, Chen K, Tamura N, Wenk H-R (2009) Evidence for residual elastic strain in deformed natural quartz. Am Mineral 94:1059-1062

Ladd MFC, Palmer RA (2003) Structure Determination by X-ray Crystallography. Kluwer Academic/Plenum Publishers, New York, 4th edition

Laetsch T, Downs RT (2006) Software for identification and refinement of cell parameters from powder diffraction data of minerals using the RRUFF project and American Mineralogist crystal structure databases. IMA General Meeting

Larson AC, Von Dreele RB (2000) General structure analysis system (GSAS). LANL Report LAUR 86-748

Le Bail A, Duroy H, Fourquet JL (1988) Ab-initio structure determination of $LiSbWO_6$ by X-ray-powder diffraction. Mater Res Bull 23:447-452

Lee J (2011) X-ray Lasers 2010. Springer, New York

Lennie AR, Laundy D, Roberts MA, Bushnell-Wye G (2007) A novel facility using a Laue focusing monochromator for high-pressure diffraction at the SRS, Daresbury, UK. J Synchrotron Radiat 14:433-438

Li W, Harrington R, Tang Y, Kubicki JD, Aryanpour M, Reeder RJ, Parise JB, Phillips BL (2011) Differential pair distribution function study of the structure of arsenate adsorbed on nanocrystalline γ-alumina. Environ Sci Technol 45:9687-9692

Lipson H, Langford JI, Hu HC (2006) Trigonometric intensity factors. International Tables for Crystallography, Vol C, p 596-598

Lutterotti L, Matthies S, Wenk H-R (1999) MAUD (Material Analysis Using Diffraction): a user friendly java program for Rietveld texture analysis and more. Proceeding of the Twelfth International Conference on Textures of Materials (ICOTOM-12), Vol. 1, 1599

March A (1932) Mathematical theory on regulation according to the particle shape and affine deformation. Z Kristallogr 81:285-297

Margaritondo G (1988) Introduction to Synchrotron Radiation. Oxford University Press, New York

Margaritondo G (2002) Elements of Synchrotron Light: for Biology, Chemistry, and Medical Research. Oxford University Press, Oxford

Müller M, Dinnebier RE, Schorr S (2011) A case study of parameterized Rietveld refinement: the structural phase transition of $CuInSe_2$ (2011) Z Kristallogr 226:956-962

Nakatsuka A, Yoshiasa A, Yamanaka T, Ohtaka O, Katsura T, Ito E (1999) Symmetry change of majorite solid-solution in the system $Mg_3Al_2Si_3O_{12}$-$MgSiO_3$. Am Mineral 84:1135-1143

Neuling HW, Schulte O, Kruger T, Holzapfel WB (1992) Texture-sensitive energy dispersive- X-ray diffraction on powders at high-pressure with synchrotron radiation. Meas Sci Technol 3:170-173

North ACT, Phillips DC, Mathews FS (1968) A semi-empirical method of absorption correction. Acta Crystallogr A 24:351-359

Nozawa S, Adachi S, Takahashi J, Tazaki R, Guerin L, Daimon M, Tomita A, Sato T, Chollet M, Collet E, Cailleau H, Yamamoto S, Tsuchiya K, Shioya T, Sasaki H, Mori T, Ichiyanagi K, Sawa H, Kawata H, Koshihara S (2007) Developing 100 ps-resolved X-ray structural analysis capabilities on beamline NW14A at the photon factory advanced ring. J Synchrotron Radiat 14:313-319

Ottonello G (1997) Principles of Geochemistry. Columbia University Press, New York

Page KL, Proffen T, McLain SE, Darling TW, TenCate JA (2004) Local atomic structure of Fontainebleau sandstone: Evidence for an amorphous phase? Geophys Res Lett 31:L24606

Pawley GS (1981) Unit-cell refinement from powder diffraction scans. J Appl Crystallogr 14:357-361

Pecharsky VK, Zavalij PY (2009) Fundamentals of Powder Diffraction and Structural Characterization of Materials. Springer, New York, 2nd edition

Post JE, Heaney PJ, Von Dreele RB, and Hanson JC (2003) Neutron and temperature-resolved synchrotron X-ray powder diffraction study of akaganeite. Am Mineral 88:782-788

Proffen T (2006) Analysis of disordered materials using total scattering and the atomic pair distribution function. Rev Mineral Geochem 63:255-274

Proffen T, Billinge SJL, Egami T, Louca D (2003) Structural analysis of complex materials using the atomic pair distribution function - a practical guide. Z Kristallogr 218:132-143

Putnis A (1992) Introduction to Mineral Sciences. Cambridge University Press, Cambridge

Ren Z, Bourgeois D, Helliwell JR, Moffat K, Srajer V, Stoddard BL (1999) Laue crystallography: coming of age. J Synchrotron Radiat 6:891-917

Ren Z, Ng K, Borgstahl GEO, Getzoff ED, Moffat K (1996) Quantitative analysis of time-resolved Laue diffraction patterns. J Appl Crystallogr 29:246-260

Rietveld HM (1967) Line profiles of neutron powder-diffraction peaks for structure refinement. Acta Crystallogr 22:151-152

Rietveld HM (1969) A profile refinement method for nuclear and magnetic structures. J Appl Crystallogr 2:65-71

Robinson I, Gruebel G, Mochrie S (2010) X-ray beams with high coherence. New J Phys 12:035002

Rodriguez-Carvajal J (1990) FULLPROF: A program for Rietveld refinement and pattern matching analysis. Abstracts of the Satellite Meeting on Powder Diffraction of the XV Congress of the IUCr, p 127

Roe RJ (1965) Description of crystallite orientation in polycrystalline materials. 3. General solution to pole figure inversion. J Appl Phys 36:2024-2031

Sabine TM (1987) A powder diffractometer for a synchrotron source. J Appl Crystallogr 20:173-178

Sarrazin P, Blake D, Bish D, Vaniman D, Collins S (1998) A miniature XRD/XRF instrument for in-situ characterization of Martian soils and rocks. J Phys IV 8:465-470

Sarrazin P, Blake D, Feldman S, Chipera S, Vaniman D, Bish D (2005) Field deployment of a portable X-ray diffraction/X-ray flourescence instrument on Mars analog terrain. Powder Diffr 20:128-133

Scarlett NVY, Madsen IC (2006) Quantification of phases with partial or no known crystal structures. Powder Diffr 21:278-284

Scherrer P (1918) Bestimmung der größe und der inneren struktur von kolloidteilchen mittels röntgenstrahlen. Nachrichten von der gesellschaft der wissenschaften zu Göttingen. Mathematisch- Physikalische Klasse 2:98

Sheldrick GM (2008) A short history of SHELX. Acta Crystallogr A 64:112-122
Snyder RL, Bunge HJ (2000) Defect and Microstructure Analysis by Diffraction. Oxford University Press
Srajer V, Crosson S, Schmidt M, Key J, Schotte F, Anderson S, Perman B, Ren Z, Teng TY, Bourgeois D, Wulff M, Moffat K (2000) Extraction of accurate structure-factor amplitudes from Laue data: wavelength normalization with wiggler and undulator X-ray sources. J Synchrotron Radiat 7:236-244
Steinhardt PJ, Bindi L (2012) In search of natural quasicrystals. Rep Prog Phys 75:092601
Stinton GW, Evans JSO (2007). Parametric Rietveld refinement. J Appl Crystallogr 40:87-95
Stout GH, Jensen LH (1989) X-ray Structure Determination: A Practical Guide. Wiley, New York
Suggit M, Kimminau G, Hawreliak J, Remington B, Park N, Wark J (2010) Nanosecond X-ray Laue diffraction apparatus suitable for laser shock compression experiments. Rev Sci Instrum 81:083902
Sutton SR (2006) User research facilities in the earth sciences. Elements 2:7-8
Tait KT, Barkley MC, Thompson RM, Origlieri MJ, Evans SH, Prewitt CT, Yang H (2011) Bobdownsite, a new mineral species from Big Fish river, Yukon, Canada, and its structural relationship with whitlockite-type compounds. Can Mineral 49:1065-1078
Tamura N, Kunz M, Chen K, Celestre RS, MacDowell AA, Warwick T (2009) A superbend X-ray microdiffraction beamline at the advanced light source. Mater Sci Eng A Struct 524:28-32
Toby BH (2001) EXPGUI, a graphical user interface for GSAS. J Appl Crystallogr 34:210-213
Toby BH, Billinge SJL (2004) Determination of standard uncertainties in fits to pair distribution functions. Acta Crystallogr A 60:315-317
Vogel S, Ehm L, Knorr K, Braun G (2002) Automated processing of 2D powder diffraction data. Adv X-ray Anal 45:31-33
Vogel SC, Knorr K (2005) Two2One - Software for the analysis of two dimensional diffraction data. Newsletter of the IUCr Commission on Powder Diffraction 32:23-25
Wang J, Toby BH, Lee PL, Ribaud L, Antao SM, Kurtz C, Ramanathan M, Von Dreele RB, Beno MA (2008). A dedicated powder diffraction beamline at the advanced photon source: Commissioning and early operational results. Rev Sci Instrum 79:085105
Wang Y, Hilairet N, Dera P (2010) Recent advances in high pressure and temperature rheological studies. J Earth Sci 21:495-516
Wang Y, Uchida T, Von Dreele R, Rivers ML, Nishiyama N, Funakoshi K, Nozawa A, Kaneko H (2004) A new technique for angle-dispersive powder diffraction using an energy-dispersive setup and synchrotron radiation. J Appl Crystallogr 37:947-956
Warren BE (1934) X-ray determination of the structure of glass. J Am Ceram Soc 17:249-254
Warren BE (1969) X-ray Diffraction Reading, MS: Addison-Wesley
Warren BE (1990) X-ray diffraction. Dover Publications, New York
Warren BE, Gingrich NS (1934) Fourier integral analysis of X-ray powder patterns. Phys Rev 46:0368-0372
Waychunas GA (2009) Natural nanoparticle structure, properties and reactivity from X-ray studies. Powder Diffraction 24:89-93
Wenk H-R, Chen K, Smith R (2011) Morphology and microstructure of magnetite and ilmenite inclusions in plagioclase from Adirondack anorthositic gneiss. Am Mineral 96:1316-1324
White CE, Provis JL, Proffen T, Riley DP, van Deventer JSJ (2010) Combining density functional theory (DFT) and pair distribution function (PDF) analysis to solve the structure of metastable materials: the case of metakaolin. Phys Chem Chem Phys 12:3239-3245
Williamson GK, Hall WH (1953) X-ray line broadening from filed aluminium and wolfram. Acta Metall 1:22-31
Yamanaka T, Ogata K (1991) Structure refinement of GeO_2 polymorphs at high-pressures and temperatures by energy-dispersive spectra of powder diffraction. J Appl Crystallogr 24:111-118
Yamashita D, Ishizaki A, Uda M (2009) Development of portable X-ray diffractometer equipped with X-ray fluorescence spectrometer and its application to archaeology. Bunseki Kagaku 58:347-355
Yang XJ, Ren Z, Moffat K (1998) Structure refinement against synchrotron Laue data: Strategies for data collection and reduction. Acta Crystallogr D 54:367-377
Young RA (1993) The Rietveld Method. International Union of Crystallography
Zelenski ME, Zubkova N, Pekov IV, Boldyreva MM, Pushcharovsky DY, Nekrasov AN (2011) Pseudolyonsite, $Cu_3(VO_4)_2$, a new mineral species from the Tolbachik volcano, Kamchatka peninsula, Russia. Eur J Mineral 23:475-481